CR-119843

71-352

HREC-6189-1
LMSC-HREC D225135-I

LOCKHEED MISSILES & SPACE COMPANY

HUNTSVILLE RESEARCH & ENGINEERING CENTER

HUNTSVILLE RESEARCH PARK

4800 BRADFORD DRIVE, HUNTSVILLE, ALABAMA

STUDY OF THERMAL CONDUCTIVITY REQUIREMENTS

VOL. I

MULTILAYER INSULATION THERMAL CONDUCTIVITY TEST PROGRAM – FINAL REPORT

June 1971

Contract NAS8-26189

Prepared for National Aeronautics and Space Administration
Marshall Space Flight Center, Alabama 35812

by

Mark J. O'Neill

A. J. McDanal

APPROVED: Juan K. Lovin

Juan K. Lovin, Supervisor
Thermal Environment Section

George D. Reny

George D. Reny, Manager
Aeromechanics Dept.

George D. Reny
for J.S. Farrior

Resident Director

FOREWORD

This report represents the results of work performed by the Thermal Environment Section of the Aeromechanics Department of Lockheed Missiles & Space Company, Huntsville Research & Engineering Center, for the National Aeronautics and Space Administration, Marshall Space Flight Center, Huntsville, Alabama, under Contract NAS8-26189. The NASA contract monitor was Mr. John Austin of the MSFC Astronautics Laboratory.

The report for "Study of Thermal Conductivity Requirements" consists of three volumes:

Volume I: Study of Thermal Conductivity Requirements — Multilayer Insulation Thermal Conductivity Test Program — Final Report - NAS8-26189

Volume II: Study of Thermal Conductivity Requirements — Multilayer Insulation Data Manual — Final Report - NAS8-26189

Volume III: Study of Thermal Conductivity Requirements — Analytical and Experimental Heat Transfer Study of a Venting Cryogen Tank — Final Report - NAS8-26189.

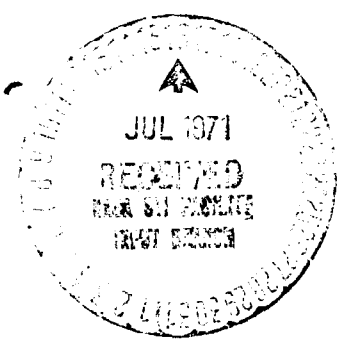

SUMMARY

A detailed parametric thermal analysis of the electrical cylindrical calorimeter was performed to identify those changes which would increase the accuracy and improve the operation of the calorimeter. A detailed description of the analysis and design improvements made in the calorimeter are discussed. Also, a complete description of the calorimeter, the calorimeter's instrumentation system and automation circuitry, the method of specimen preparation and the environmental control apparatus is included.

A detailed discussion of the thermal conductivity test procedure, compression test procedure and the method for obtaining physical density data is presented. Using double-aluminized mylar and Tissuglas composite as an example, the procedure for the presentation of the total data matrix of this multilayer insulation (MLI) is given.

Thermal conductivity and compression tests were conducted for six multilayer insulation materials to obtain temperature-dependent thermal conductivity data and compressibility versus layer density data. By mutual agreement with the Contracting Officer's Representative the materials tested were:

1. Double-aluminized mylar and Tissuglas
2. Double-aluminized mylar and Goodyear Aerospace Company (GAC)-9 white foam
3. Double-aluminized mylar and dacron net
4. Superfloc
5. Double-aluminized mylar and Nomex Net
6. Double-aluminized mylar and Cerex* spunbond nylon.

*Cerex is a registered trademark for spunbonded nylon material manufactured by Monsanto Company.

The thermal and compression data obtained during the test program were used to prepare the following curves for each material over a wide range of layer densities and temperatures:

- Layer density versus physical density
- Thermal conductivity carpet plots which present thermal conductivity as a function of layer density and temperature
- Density times thermal conductivity carpet plots which present density-conductivity product as a function of layer density and temperature
- Layer density versus compression.

Data generated during this test program are compiled in a separate multilayer insulation data manual.* The data manual includes a brief description of the materials tested, method of specimen preparation, the test procedure and error analysis, while this report gives a precise treatment to each item. The purpose of the data manual is to present design engineers with experimental data for use in designing MLI space thermal control systems. The contents are comprehensive with regard to the variety of insulation composites, the parameters which can be varied and the range of the parameters.

Empirical correlations were developed which fit the previously defined surfaces (carpet plots). They present thermal conductivity and density times thermal conductivity as functions of temperature and layer density. The technique used in developing these correlations is discussed in Section 3. The correlations are presented in the data manual for all insulations tested.

An analytical and experimental study was conducted to develop a new multilayer insulation composite by utilizing a net spacer which is as nearly optimum a spacer as possible. The net spacer selected is Cerex spunbond nylon developed by Monsanto. Results of the study are presented in this report.

*Volume II of this document.

The results of the error analysis discussed in Section 5 verify the accuracy and utility of the data generated by the cylindrical calorimeter. An average probable error of $\pm$ 2.10% was determined for all data points obtained during the test program. Each data point taken during the test program was individually analyzed to determine where inaccuracies occur and how they can be eliminated.

In order to experimentally verify the accuracy of thermal conductivity measurement with the cylindrical calorimeter, repeatability tests were conducted for several data points. The demonstrated repeatability was excellent, verifying the accuracy found in the error analysis.

CONTENTS

LIST OF ILLUSTRATIONS

NOMENCLATURE

Symbol	
A	total insulation surface area
C_p	specific heat
D	calorimeter tube diameter
I	test section current
K	thermal conductivity
ℓ	layers
L	calorimeter test section length
m	mass
$\bar{N}$	layer density
P	test section power
q	heat flux through insulation on test section
r	calorimeter tube radius
t	calorimeter tube thickness
T	temperature
V	test section voltage
w	weight

Greek	
$\Delta\bar{N}$	change in layer density
ΔT	temperature differential through insulation
ϵ	emissivity
ρ	physical density of insulation

Subscripts

a	allowable (q_a is allowable heat flux)
i	inside of insulation
o	outside of insulation
r.s.	reflective shield
s	spacer

Section 1
INTRODUCTION

In 1967, Lockheed-Huntsville designed and fabricated for NASA-MSFC the first electrical cylindrical calorimeter for measuring temperature-dependent thermal conductivity of multilayer insulation composites. Although the data obtained on earlier calorimeters were accurate, many refinements and design improvements were necessary to meet the increasing demand for inexpensive and accurate design data for MLI thermal control systems.

Accurately determined temperature dependent and layer density dependent design data must be generated to meet the needs of an MLI design engineer for all conceivable design requirements. Experimental data must be comprehensive enough to provide a complete picture of the total required range of layer densities at the total required range of temperatures. Lockheed-Huntsville's electrical cylindrical calorimeter has the capability to generate test data within this required range.

The results of the complete analytical and experimental study are presented in three volumes. This report (Volume I) documents the analytical study performed and presents specific examples of test data obtained during the test program. A special need was felt for presenting density, compression and thermal conductivity test data in a design data manual. Volume II presents all design data obtained in a form well suited for design engineers. Volume III documents the results of an actual MLI application. An MLI composite is applied to a venting cryogen storage tank, and experimental studies are performed.

Section 2
CALORIMETER ANALYSIS AND DESIGN IMPROVEMENTS

2.1 CALORIMETER THERMAL ANALYSIS

A parametric thermal analysis of the cylindrical calorimeter was performed. Three parameters were studied: inside tube diameter, wall thickness, and internal emissivity. The nodal network is shown in Fig. 1. The nodes are sufficiently small to yield accurate temperature and heat rate data. All conduction resistances were input as functions of temperature for accuracy. Experimental data were used for the material conductivities. The internal radiation resistors were calculated to take multiple reflections into account, as well as standard diffuse emission. A room-temperature data point was simulated in all cases.

Figures 2, 3 and 4 present the results of the analysis. In each of these figures, the ordinate represents the temperature difference, $T_{\text{node 82}} - T_{\text{node 85}}$. The abscissa represents the percent error in conductivity measurement which is defined by the following equation:

$$\% \text{ Error} = \frac{\text{Measured K} - \text{Actual K}}{\text{Actual K}} \times 100\% .$$

The reason for presenting the results in this fashion is that the error is not only a function of geometry, but also of longitudinal gradient $(T_{82} - T_{85})$.

In Fig. 2, the error is shown for different thicknesses and diameters with the internal emissivity fixed as zero. At first glance, it appears unusual that the error is not zero for a zero longitudinal gradient $(T_{82} - T_{85})$. However, upon inspection of the temperature distributions, it was found that when the longitudinal gradient is zero along the calorimeter, the longitudinal gradient in the MLI specimen is not zero. Even more interesting is the fact that when

the longitudinal gradient becomes slightly negative ($T_{85} > T_{82}$), the gradient in the MLI is oppositely directed (the outer layers of MLI above node 82 are hotter than those above node 85). The result of these oppositely directed gradients is heat flow in one direction in the calorimeter, and heat flow in the opposite direction in the outer layers of MLI. The error is zero when these two heat flows balance one another in magnitude.

With the real calorimeter, the longitudinal gradient is maintained at $0 \pm 0.02^{\circ}F$ between nodes 82 and 85. The $\pm 0.02^{\circ}F$ band is shown in Fig. 2 as dashed vertical lines. Regardless of thickness or diameter, it can be seen that the error for this zero emissivity case is less than 1.5% when the longitudinal gradient remains within the $\pm 0.02^{\circ}F$ band.

Figures 3 and 4 present results for emissivities of 0.5 and 1.0, respectively. It is obvious from the figures that radiation has a huge effect on the error. As the longitudinal gradient increases in magnitude (regardless of sign), the error rises drastically. This increase in error is due to relatively large amounts of radiation heat transfer inside the calorimeter. The error is slightly greater for the $\epsilon = 1.0$ case than for the $\epsilon = 0.5$, as would be expected.

Tube wall thickness still has no appreciable effect, but diameter has a large effect in these two radiation cases. In Figs. 3 and 4, it is easily seen that the larger the diameter, the larger the error. This is due to an increase in both area and view factor for larger diameters, resulting in more radiation heat transfer along the calorimeter.

From the computer thermal analysis, the following conclusions were drawn:

1. The internal emissivity should be as close to zero as possible;
2. The diameter should be as small as practical;
3. Because wall thickness has no appreciable effect on the longitudinal heat flow error, the wall should be made as thin as practical to minimize heat storage error.

The calorimeter was designed on the basis of these conclusions. The table below shows the changes in the new calorimeter compared to the old calorimeter.

Parameter	Old Calorimeter	New Calorimeter
D	3.0	2.5
t	1/16	1/32
ϵ	0.8 - 0.9	0.03 (aluminized mylar)
Material	Silicone Fiberglas	Phenolic Fiberglas (lower ρ,K,C_p)

2.2 CALORIMETER DESCRIPTION

Lockheed-Huntsville's electrical cylindrical calorimeter consists of a phenolic glass fiber tube, 39 inches long, 2.5 inches outside diameter and 1/32 inch thick as shown schematically in Fig. 5. Six-mil copper magnet wire is wound continuously around the tube to form three individual heaters. There are no spacings between either the adjacent windings or the heaters. The result is that 38 inches of uniform, continuous windings completely cover the base cylinder. As shown in Fig. 5, the center heater, which is 36 inches long, serves as the "test heater." It is flanked on either side by a one-inch long end heater. Separate power control is provided for each heater in order to provide for a uniform temperature distribution along the tube. The center test heater is automated and is designed to maintain a constant temperature at the center of the calorimeter. The end heaters are maintained at a slightly higher temperature than the test heater to reduce longitudinal heat loss.

2.3 CALORIMETER INSTRUMENTATION SYSTEM

The temperature sensing devices used on the calorimeter are mainly copper constantan thermocouples. Differential thermocouples of 3-mil copper and constantan wire measure temperature differences between the following pairs of points (Fig.5): 1 and 2, 2 and 4, 3 and 4, 4 and 5, 4 and 6 and 6 and 7.

A platinum resistance thermometer is used to measure the aboslute temperature at point 4. A reserve copper-constantan absolute thermocouple is also located at point 4, in case of malfunction of the resistance thermometer.

There are three main improvements in the new instrumentation system over past systems: (1) the platinum resistance thermometer is more sensitive than the thermocouple it replaces. This allows determination of temperature changes with time in a shorter period of time, which allows power corrections to be made more accurately and more often, thereby expediting data point acquisition; (2) the new system has seven temperature-measurement locations along the calorimeter rather than five as used previously. This provides more information concerning the lengthwise temperature gradient than before, and if one thermocouple malfunctions, the test can continue by using the thermocouples closest to it to monitor the lengthwise gradient; and (3) all absolute thermocouples are referenced to a ConOhmic thermocouple reference junction oven in the new system, rather than being referenced to LN_2 as in the past. The boiling temperature of LN_2 fluctuates with barometric pressure, while the oven is electrically maintained at a constant temperature. These improvements further increase the accuracy of the new calorimeters.

2.4 CALORIMETER AUTOMATION CIRCUITRY

A new automated circuitry controls the power input to the calorimeter. The circuitry is simpler than past circuitry because the longitudinal heaters have been eliminated. The basic automation system is composed of the test heater automation circuit and two end-heater automation circuits.

The test heater automation circuit is designed to maintain a constant temperature at the center of the calorimeter (point 4 in Fig. 5). The circuit utilizes a VECO synchronous controller which balances the voltage from the platinum resistance thermometer with a reference voltage, and the inbalance between these voltages is amplified and used to power the test heater. The controller allows the test heater to be maintained within $1/200^{\circ}F$ in the range

of testing (i.e , -200°F to +200°F). Because of the extreme accuracy of the synchronous controller power oscillations with time are negligible so that it is not necessary to convert from automatic to fixed power when thermal stabilization is achieved as in past procedures. The primary benefit of this new automation circuit is the elimination of personnel attendence during the stabilizing period (which lasts approximately 18 hours).

The end heater automation circuits maintain a slightly higher temperature at the end than at the next thermocouple location inward. The right end circuit maintains point 7 (Fig. 5) at a temperature slightly higher than point 6. The left end circuit maintains point 1 at a temperature slightly higher than point 2. There are differential thermocouples between points 1 and 2 and between points 6 and 7. The voltages from these thermocouples are amplified and used to power the end heaters. By means of a variable potentiometer, the temperature difference can be set at any reasonable value. The end heater automation circuits are essentially the same as in the past, with a few refinements to allow more power capability and more stable amplification.

2.5 SPECIMEN PREPARATION

The entire calorimeter is wrapped with a specimen of the MLI composite to be tested. The longitudinal portion of the calorimeter is wrapped circumferentially and the ends are covered with circular pieces of insulation. Figure 6 shows that the longitudinal portion of the specimen joins the "end caps" at a 45-degree diagonal joint. This eliminates any thermal shorting between layers. Heat loss is, therefore, limited to that which passes through the instrumentation wires and nylon support cords which exit the test specimen at the 45-degree joint. This heat loss is compensated by the automated end heaters.

After the calorimeter is wrapped at a predetermined layer density, a 3-mil copper constantan differential thermocouple is attached to the outside of the insulation to measure the temperature difference through the insulation. The entire package is then suspended in the chamber by the support rod and support brackets (Fig. 7). The shroud and chamber are then closed and testing is begun.

2.6 ENVIRONMENTAL CONTROL APPARATUS

To support previous MLI contracts, Lockheed-Huntsville constructed a vacuum chamber for conducting thermal conductivity tests on MLI systems. T' e chamber was designed specifically to meet the requirements of the thermal tests with the two primary criteria: (1) precise thermal control, and (2) speed of operation. This chamber is shown in Fig. 7. The nominal dimensions are 17.5 in. inside diameter and 52 in. long. The chamber was constructed by butting a stainless steel, right circular cylinder chamber 23 in. long, against a glass bell jar chamber 30 in. long. An aluminum shroud 14 in. inside diameter and approximately 47 in. long is wrapped with heater wire to provide a controllable thermal environment for the test specimen. A copper coil encloses the aluminum shroud, and LN_2 is circulated through the coil for thermal control of the shroud. The shroud and coil are enclosed in an MLI blanket to minimize heat leakage between the shroud and the chamber.

A new and improved shroud heating and cooling system was designed. Previously, hot fluids (liquids or air) have been used for heating the copper coil shroud to provide the external temperature environment for the calorimeter for "hot" data points. An on/off cyclic flow of LN_2 in the coils was used for "cold" points. In the past, these systems were adequate, but far from optimum. With the redesign of the calorimeters for greater accuracy, the need for a more accurate external thermal environment system is evident.

Figure 7 is a schematic showing the new shroud heating and cooling system. Surrounding the calorimeter is a 20-mil aluminum shroud which is wound with heater wires. This electrical heater is controlled by a VECO synchronous controller, which maintains the heater at any desired temperature from -220 to 180°F. At "hot" data points, this heater is used alone to control the temperature of the calorimeter external environment. For cold points, the heater is used in combination with the cooling coils (Fig. 7) in the following way. The synchronous controller is also capable of controlling LN_2 flow. Therefore, a desired temperature is set on a calibrated potentiometer. When the temperature of the heater is above this prescribed temperature, the controller opens

a valve allowing LN_2 to flow through the coils until a temperature slightly below the desired temperature is achieved at the aluminum heater shroud. The LN_2 is then shut off by the controller. If the temperature falls slightly, the heater is activated by the controller. With this dual electrical heater/ LN_2 coil system, the temperature of the calorimeter external environment remains at the prescribed temperature within ± 1 to $2^{\circ}F$ over the full temperature range -220 to $180^{\circ}F$. This represents a great improvement in accuracy over the previous non-electrical systems.

Section 3
EXPERIMENTAL METHODS, DATA PRESENTATION, AND SEMIEMPIRICAL CORRELATIONS

3.1 THERMAL CONDUCTIVITY TESTING

The initial step in thermal conductivity testing is to select the MLI material. After the material has been selected, the calorimeter is carefully wrapped at the required layer density and compression. The fully insulated calorimeter is then installed inside the shroud in the vacuum chamber. The chamber is evaluated to a pressure of $\leq 8 \times 10^{-6}$ torr by both a mechanical pump and a diffusion pump. The pressure inside the vacuum chamber is measured by an ion pressure gage. The calorimeter is then heated or cooled to the desired temperature either by supplying power to the shroud heater or by cooling the shroud with liquid nitrogen. When the calorimeter attains the desired temperature, the inside is heated to a slightly higher temperature than the outside by supplying power to the calorimeter test heater. A temperature drop of approximately $40^{\circ}F$ is usually desired across the insulation. The automated end heaters maintain a slightly higher temperature at the ends than the test heater to compensate for longitudinal heat loss out the ends. Sections 2.4 and 2.6 describe the automatic circuitry that maintains the shroud temperature, calorimeter temperature and temperature differential across the insulation at the prescribed values.

When the temperature of the calorimeter is constant with time, and the temperature gradient along the test heater is zero, steady state has been achieved. When steady state is reached, power and temperature distributions along the calorimeter are constant. With such a distribution the test section of the calorimeter very accurately approximates a section of an infinite cylinder.

The solution to the heat conduction equation for radial heat flow through an infinite cylinder is given on the following page:

$$K(T) = \frac{q \ln \left(\frac{R_o}{R_i}\right)}{2\pi L (T_i - T_o)} \quad (1)$$

where

$$T = \frac{T_o + T_i}{2} \quad (2)$$

is the mean temperature through the insulation. The parameters r_o, r_i, L, T_o and T_i are measured directly while q is the power input to the calorimeter. That is

$$q = P = IV. \quad (3)$$

Therefore, by solving Eq. (1), thermal conductivity as a function of mean insulation temperature is found. Table 1 presents the thermal data obtained by the procedure outlined above for DAM/Tissuglas.

3.2 COMPRESSION TESTING

Using the apparatus of Fig. 8, compression tests for MLI composites are performed in the following manner:

1. The MLI material under study is cut into 10 x 10-inch squares.
2. One-half of the squares are stacked and thickness measurements with no applied load are made (Fig. 8a). Five measurements are made: four, two inches in from each side and the fifth at the center. The measurements are averaged to obtain the stack thickness. The layer density is established by dividing the known number of layers by the stack thickness.
3. A plate weighing 49 grams is placed on the stacked layers (Fig. 8b) and the five measurements as in (2) above are made. The plate thickness is then subtracted from each measurement, the values are averaged and, with the number of layers known, the layer density is established.
4. The plate is removed and the remaining layers of the MLI are stacked. Measurements with no load, 49, 279, 1147, and 4815 grams are made in the same manner as (2) above.

The total compression exerted on the stacked layers is due to the weight of the applied load and the weight of the MLI. Since the load due to the MLI's weight varies linearly from the top of the stack to the bottom, the mean self-loading corresponds to 1/2 the total MLI weight. To obtain data at a very low compressive load, it is therefore necessary to work with very few layers. This is the reason for obtaining data with only half of the layers before going to the main test series with all the layers. As an example, the compression data for DAM/Tissuglas is presented in tabular form (Table 2) and graphical form (Fig. 9). The number of layers used in each case is indicated in Table 2. One layer represents one reflector shield and one spacer (where spacers are used).

3.3 PHYSICAL DENSITY MEASUREMENT

The physical density for a MLI composite is obtained by weighing several 10 x 10-inch squares of the reflector shield and the spacer. From this, an average mass of one 10 x 10-inch sample of the reflector shield and spacer is found. These values are substituted into the following equation

$$\rho = \frac{(\bar{N}+1)\, m_{r.s.} + (\bar{N})\, m_s}{\text{Area}}$$

where

$m_{r.s.}$ = average mass of one 10 x 10-inch reflective shield

m_s = average mass of one 10 x 10-inch spacer

Area = 100 in^2

$\bar{N}$ = layer density in layers/in.

Table 3 presents density data for DAM/Tissuglas. Figure 10 presents the same data in graphic form.

3.4 METHOD OF PRESENTING DATA

For each MLI tested, 12 thermal conductivity data points are obtained. Four temperature points for each of three layer densities are taken, using a small temperature drop ($< 50^{\circ}F$) to assure temperature dependence.

The data matrix obtained for each MLI material tested is shown qualitatively in Fig. 11. The thermal conductivity (K) of each MLI can be described as a function of two variables, temperature (T) and layer density ($\bar{N}$). This functional relationship can be shown graphically as a surface, $K = f(T, \bar{N})$, in $K\text{-}\bar{N}\text{-}T$ space. Testing is conducted over a range of temperatures (T-range) from $-200^{\circ}F$ to $+200^{\circ}F$, and over a range of layer densities ($\bar{N}$-range) from a minimum practical density to a highly compressed layer density. The twelve data points obtained for each MLI define the K-surface, as shown in Fig. 11. Another data surface obtained in the $\rho K = f(\bar{N}, T)$ where ρK is the density-conductivity product. The K and ρK data surfaces are presented in carpet plot form for DAM/Tissuglas in Figs. 12 and 13 respectively.

The presentation of MLI thermal conductivity data in carpet plot form is an innovation developed during this study. Since MLI thermal conductivity is a function of the two independent variables, temperature and layer density, the data can be presented in carpet plot form which allows exact double interpolation to determine the value of conductivity for any set of (T, $\bar{N}$) within the ranges of the data. Presentation of the data as a family of curves would not allow accurate and easy double interpolation. For a detailed description and example of the use of the carpet plot, the reader should consult Appendix A. Density times thermal conductivity (ρK) data is also presented in carpet plot form.

The data in Figs. 9 through 13 can be combined to yield carpet plots showing conductivity and density-conductivity product as function of temperature and compressive load, but these plots have been found to be difficult to use due to intersection of isotherms when plotted. An alternate approach is suggested to obtain these data. As an example, if the conductivity is needed for a certain compressive load and temperature, use Fig. 9 to obtain the layer density corresponding to the compressive load in question. Then use Fig. 12, with this layer density and the original temperature as coordinates. Determining the conductivity (or the density-conductivity product) in this two-step process has been found to be easier than using a carpet plot with compressive load and temperature as the coordinates.

Density times thermal conductivity data are presented due to the extreme importance of the ρK product in multilayer insulation design work for weight limited applications. Presentation of data in ρK form is duly justified by the derivation shown below.

For most weight-limited MLI system applications the following variables are fixed:

$\Delta T = T_i - T_o$ (temperature differential through the insulation)

A = total surface area

q_a = allowable heat transfer.

The conduction equation for this process is

$$q_a = \frac{K A \Delta T}{t} \tag{4}$$

where t is the insulation thickness. Solving this equation for t gives

$$t = \frac{K A \Delta T}{q_a} \quad . \tag{5}$$

The weight of the MLI system is:

$$w = \rho A t \tag{6}$$

where w is the weight and ρ is the physical density of the MLI. Substituting Eq. (5) into this equation yields:

$$w = \rho A \left(\frac{K A \Delta T}{q_a} \right) \quad . \tag{7}$$

Rearranging:

$$w = \rho K \left(\frac{A^2 \Delta T}{q_a} \right) \quad . \tag{8}$$

Since the term in parenthesis is a constant quantity,

$$w = \rho K \times \text{constant} \tag{9}$$

and ρK is seen to be the parameter to minimize for weight limited applications.

3.5 SEMIEMPIRICAL CORRELATION DEVELOPMENT

A total of twelve data points form the $K = f(T, \bar{N})$ and $\rho K = f(T, \bar{N})$ surfaces in Fig. 12 and Fig. 13. A curve fitting technique is applied to this surface to develop a semiempirical correlation in variables T and $\bar{N}$ that completely defines the K and ρK surfaces within the range of testing. A five-term polynomial is used with experimentally determined values of T, $\bar{N}$ and K to form a 5 x 5 system of linear equations. The five-term polynomial is of the form

$$K = \frac{AT^3}{N} + BT + CT^2 + DN + EN^2 \tag{10}$$

where T is the mean temperature at which each data point is taken, $\bar{N}$ is the layer density and K is the corresponding value of thermal conductivity. The solution of the 5 x 5 system gives 5 constants (A through E) for the surface under consideration. The semiempirical correlation for the K-surface of DAM/Tissuglas is

$$K \times 10^5 = (1.4271 \times 10^{-5})\frac{T^3}{\bar{N}} - (2.1744 \times 10^{-2})T + (1.8431 \times 10^{-5})T^2 + (2.2822 \times 10^{-2})\bar{N} + (2.2881 \times 10^{-5})\bar{N}^2. \tag{11}$$

Similarly, for the ρK surface

$$\rho K \times 10^5 = \left[0.0226\,\bar{N} + 0.0212\right]\left[(1.4271 \times 10^{-5})\,\frac{T^3}{N} - (2.1744 \times 10^{-2})\,T + (1.8431 \times 10^{-5})\,T^2 + (2.2822 \times 10^{-2})\,N + (2.2881 \times 10^{-5})\,\bar{N}^2\right]$$

[Units: T ($^\circ$R), $\bar{N}$ (ℓ/in.), K (Btu/hr-ft-$^\circ$F), ρ (lbm/ft^3)].

Section 4
NET SPACER STUDY

Analytical and experimental investigations were performed to develop a new MLI composite by utilizing a net spacer which is as nearly optimum a spacer as possible. A comprehensive survey of existing nets was made. Materials investigated in the survey included nylon, silk, dacron and glass fibers. Net spacer parameters considered were:

- Fiber material
- Thickness
- Percent cutout
- Fiber size
- Weave spacing
- Weave geometry
- Fiber construction
- Material bulk thermal conductivity
- Material bulk density
- Compressibility
- Outgassing in vacuum
- Sheet strength
- Coefficient of thermal expansion.

Cerex spunbonded nylon was the material chosen due to an examination of all of the above parameters. One of the most important and influencing parameters involved in the selection was the strength and fabricability properties of the Cerex. At the time of the study Cerex was not a production item.

Cerex spunbonded nylon developed by Monsanto Company is manufactured in several sheet thicknesses and sheet densities. The minimum sheet thickness and density were selected because for most weight-limited MLI system applications ρK is the parameter that should be minimized. As spacer thickness

decreases, the attainable layer density increases. Large layer densities (without being achieved by simply compressing the composite) are desirable since the radiation heat transfer contribution is inversely proportional to layer density.

Cerex spunbonded nylon is uniquely constructed by placing nylon fibers in a high-temperature air stream and allowing the fibers to be blown against a screen. The fibers are fused together due to the high temperature air stream which is at the approximate melt temperature of the fibers. This construction technique creates a random weave geometry and weave spacing for the Cerex. This random weave spacing also affects the percent cutout. Some intermediate optimum value of the weave spacing exists for a given fiber diameter, since values that are too small result in small percent cutouts, and values that are too large result in touching the radiation shields. The percent cutout for Cerex ($\sim 90\%$) was large enough to keep physical density at values comparable to other net spacers, yet small enough that there could be no contact between radiation shields.

In most net spacers, various weave patterns are available: square, rectangular, hexagonal, octagonal and others, but these spacers are severely limited in strength properties. For example, a square weave pattern is used in the dacron net spacer. If a tensile force is exerted in a diagonal direction, the dacron net loses its strength properties and deforms continuously. With the Cerex, there is no diagonal direction due to the random weave pattern. Therefore, Cerex's strength properties are uniform in all directions. This uniformity in strength allows greater ease in handling the material and fabricating the test specimens. None of the previous net spacers tested to date have had this extremely important combination of uniform strength properties and ease in fabricability which is most desirable.

MLI composites have various applications. One important use is in the insulation of cryogen storage tanks where lateral strength of the spacer and ease in fabricability of the composite are of utmost importance. Spacers such

as Tissuglas have excellent thermal properties but will probably never be used due to the extremely fragile nature of the material. The DAM/GAC-9 white foam composite also has favorable thermal properties but the while form is semirigid and fabricability is a problem. Dacron nets and Nomex nets are limited due to deformation which occurs when the material is handled. In comparison, DAM/Cerex spunbonded nylon is a composite having good thermal properties and excellent fabricability characteristics.

Low values of material thermal conductivity, and coefficient of thermal expansion were found for Cerex, because of its nylon composition. A minimum value for the thermal conductivity parameter is desirable to prevent heat conduction through the material. Due to the nature of previous nylon net spacer materials, outgassing problems have occurred because of the use of the preservative, formaldehyde, in manufacturing the material. With Cerex, no outgassing problems were encountered primarily because formaldehyde is not used in manufacturing the material.

The experimental portion of the net spacer study involved density measurements, compression tests and thermal conductivity tests performed on the MLI composite of double-aluminized mylar and Cerex spunbonded nylon. The results of the experimental work presented in tables and graphs show that this MLI composite compares well with other similar composites. The total data matrix is given as follows:

Table 4	Thermal Data
Table 5	Compression Data
Table 6	Density Data
Figure 10	Layer Density vs Physical Density
Figure 14	Layer Density vs Compression
Figure 15	Thermal Conductivity Carpet Plot
Figure 16	Density Times Thermal Conductivity Carpet Plot.

To compare the DAM/Cerex composite with other similar MLI composites refer to the Data Manual – Volume II, which presents thermal design data for six MLI.

Section 5

CALORIMETER ACCURACY, ERROR ANALYSIS AND REPEATABILITY TESTING

5.1 CALORIMETER ACCURACY AND ERROR ANALYSIS

Thermal conductivity data obtained from the calorimeter are verified by error analysis for each data point obtained. To determine the error in thermal conductivity it is necessary to determine the error introduced by heat storage, longitudinal heat loss and physical measurements. The Kline-McClintock probable error analysis procedure is used to obtain the combined effects of the errors on thermal conductivity. Hale* gives a precise treatment of the error analysis.

Results of the error analysis verify the extreme accuracy of the calorimeter for obtaining thermal conductivity data. An average probable error of $\pm 2.10\%$ was found for all data points obtained during the test program. This average probable error of $\pm 2.10\%$ represents a substantial increase in accuracy over past calorimeter data due primarily to increased sensitivity in the instrumentation system and the improvements in physical design of the calorimeters. Accuracy has been increased by the addition of a platinum thermometer. A temperature of $1^{\circ}F$ is equivalent to 100 μV output from the platinum thermometer, while $1^{\circ}F$ is equivalent to approximately 20 μV output (at room temperature) from an absolute copper-constantan thermocouple which is replaced. Also, the ConOhmic thermocouple reference junction oven represents a definite improvement over past procedures of referencing the absolute thermocouples to a liquid nitrogen bath.

*Hale, D. V., and M. J. O'Neill, "Study of Thermal Conductivity Requirements," LMSC-HREC D162128, Lockheed Missiles & Space Company, Huntsville, Ala., February 1970.

Cost in data point acquisition has been reduced due to greater speed in stabilizing on steady state power. This reduced time is due primarily to the increased sensitivity of the platinum thermometer used in measuring absolute calorimeter temperature and design improvements in the automation circuitry.

Results of the error analysis for DAM/Tissuglas at a layer density of 200 layers/in. are presented in Table 7. As stated previously, the total percentage of probable error is due to the percentage of error attributable to the heat stored in the calorimeter tube, the percentage of error due to the quantity of heat loss out the ends of the calorimeter and the percentage of error introduced by physical measurements. Table 7 gives an indication of the relative contribution of each of the three component errors to the total probable error. Factors such as heat loss out instrumentation lead wires, heat loss out insulation joints and instrumentation access openings and longitudinal heat loss by tunnel radiation within the calorimeter can cause errors in test data. Errors currently resulting from these factors are not detrimental to the test results.

5.2 REPEATABILITY TESTING

In order to experimentally verify the accuracy of the calorimeter, a series of repeatability tests was conducted. As part of the original test program thermal conductivity tests of DAM/Cerex at layer densities of 75, 100 and 150 were conducted. Three data points for each layer density were obtained.

The repeatability test was initiated after all testing of the DAM/Cerex was completed. After the final data point for this insulation was obtained the test specimen at a layer density of 75 layers/in. was removed from the vacuum chamber, subjected to atmospheric conditions for a period of 18 hours and then replaced inside the vacuum chamber. No deviations from original thermal conductivity test procedure were made.

Results of the repeatability test are presented in Table 8. Included in the table is the percentage of probable error for each data point obtained in

the original test and the repeat test. For all three data points obtained, the percentage difference in thermal conductivity was within the probable error band determined by error analysis. The results are presented graphically as thermal conductivity vs temperature in Fig. 17.

The results of the repeatability test and error analysis again identify the electrical cylindrical calorimeter as an extremely accurate and useful tool in obtaining thermal conductivity data.

Section 6
CONCLUSIONS AND RECOMMENDATIONS

The following general conclusions are drawn from the study:

1. The new calorimeters operated with unprecedented accuracy. The average probable error for the 72 data points obtained was just $\pm 2.10\%$. The repeatability tests experimentally substantiated this extreme accuracy.

2. The new automation system functioned with great ease and economy. The data point conditions were simply dialed in with variable resistors, and within an average of two days the data point was acquired. Only minimal personnel attention was required for data acquisition.

3. The entire data acquisition system functioned with reliability. The system operated 24 hours a day, seven days a week for the last seven months of the study without any noteworthy problems.

4. The method of presenting MLI data in carpet plot form was developed and proved to be superior. By double interpolation on the carpet plots, K or ρK data can be obtained easily and accurately for any given set of ($\bar{N}$, T) or (compressive load, T).

5. A new and untried spacer material, Cerex, was located and tested with encouraging results. The competitive thermal properties, coupled with the exceptional strength and fabricability of the new material, make the new composite extremely attractive.

6. Accurate temperature and layer density dependent thermal design data were obtained for six different MLI composites.

Specific recommendations based on the results of the study are:

1. Data should be obtained for K and ρK as functions of temperature and layer density and as functions of temperature and compression for other MLI composites not studied under this contract. The data should be presented in the newly developed carpet plot form.

2. The proven concept of MLI cylindrical calorimetry should be expanded to include the capability of testing space shuttle materials. The temperature ranges for such materials will have higher limits (350° to 400°F), but such a capability could be easily developed by modifying the existing cylindrical calorimetry facilities.

3. Effort should be continued in developing new MLI materials, such as Cerex, especially new materials with space shuttle capabilities. The continued effort will undoubtedly lead to new and greatly superior materials for space thermal control systems.

Table 1

THERMAL DATA FOR DAM/TISSUGLAS

Layer Density $\bar{N}$ (layers/in)	Chamber Pressure (torr)	ΔT (^{o}F)	Mean Temperature (^{o}F)	Thermal Conductivity ($K \times 10^{5}$) (Btu/hr-ft-^{o}F)	Density x Thermal Conductivity ($\rho K \times 10^{5}$) (Btu/hr-ft-^{o}F) x (lbm/ft^{3})	Probable Error $\pm$ (%)
120	7.0×10^{-7}	40.2	-198.1	0.77	2.13	1.02
120	3.4×10^{-7}	35.0	- 60.5	3.16	8.72	1.15
120	4.0×10^{-7}	31.9	66.9	12.60	34.78	1.32
120	5.2×10^{-6}	29.0	191.1	29.50	81.42	1.40
160	1.0×10^{-7}	38.2	-199.6	1.41	5.19	1.03
160	9.4×10^{-8}	42.1	- 53.4	3.62	13.32	0.896
160	1.2×10^{-7}	38.5	68.7	12.04	44.31	1.19
160	1.9×10^{-6}	36.5	195.0	20.95	77.10	1.90
200	9.0×10^{-8}		-198.2	2.33	10.72	1.11
200	9.0×10^{-8}		- 72.6	2.68	12.33	1.16
200	2.2×10^{-7}		94.8	5.65	25.99	1.59
200	4.0×10^{-6}		200.1	19.65	90.39	3.16

Table 2

COMPRESSION DATA FOR DAM/TISSUGLAS

Number of Layers	Layer Density (Layers/in)	Mechanical Load (lb/in^2)
90	149	0.00054
90	183	0.00162
90	235	0.00668
90	275	0.0258
90	351	0.113

Table 3

DENSITY DATA FOR DAM/TISSUGLAS

Layer Density $\overline{N}$ (Layers/in)	Physical Density ρ (lbm/ft^3)	Physical Density Equation
120	2.79	$\rho = 0.0226\ \overline{N} + 0.0212$
160	3.69	
200	4.60	

Table 4

THERMAL DATA FOR DAM/CEREX

Layer Density $\overline{N}$ (layers/in)	Chamber Pressure (torr)	ΔT (^{o}F)	Mean Temperature (^{o}F)	Thermal Conductivity ($K \times 10^{5}$) (Btu/hr-ft-^{o}F)	Density x Thermal Conductivity ($\rho K \times 10^{5}$) (Btu/hr-ft-^{o}F) x (lbm/ft^{3})	Probable Error $\pm$(%)
75	3.5×10^{-6}	41.0	-190.1	2.29	8.27	1.45
75	5.6×10^{-6}	50.3	0.4	4.42	15.97	1.63
75	6.0×10^{-6}	36.9	198.8	13.03	47.07	1.87
100	1.4×10^{-8}	40.4	-186.8	3.10	14.91	1.91
100	1.0×10^{-7}	43.9	7.2	5.11	24.58	1.90
100	2.4×10^{-6}	29.7	194.0	18.49	88.92	2.23
150	*$\leq 8.0 \times 10^{-6}$	32.2	-182.1	4.21	30.33	2.78
150	*$\leq 8.0 \times 10^{-6}$	35.6	- 17.8	7.07	50.93	2.78
150	*$\leq 8.0 \times 10^{-6}$	27.5	198.8	23.54	169.56	2.86

*Exact pressure reading was not obtained due to faulty pressure gage.

Table 5

COMPRESSION DATA FOR DAM/CEREX

Number of Layers	Layer Density (Layers/in)	Mechanical Load (lb/in^2)
25	81.2	0.000352
25	120.8	0.00143
50	93.6	.000699
50	122.2	0.00178
50	167.8	0.00684
50	196.9	0.0260
50	237.0	0.107

Table 6

DENSITY DATA FOR DAM/CEREX

Layer Density $\overline{N}$ (Layers/in)	Physical Density (lbm/ft^3)	Physical Density Equation
75	3.61	$\rho = 0.0479\,\overline{N} + 0.212$
100	4.81	
150	7.21	

Table 7

RESULTS OF THE ERROR ANALYSIS FOR DAM/TISSUGLAS AT $\bar{N}$ = 200 ℓ/IN

Mean Temp (^{o}F)	% Storage Error ± (%)	% Longitudinal Heat Loss Error ± (%)	% Measure-ment Error ± (%)	Probable Error ± (%)
-198.2	0.206	0.0042	1.09	1.11
- 72.6	0.389	0.0082	1.09	1.16
94.8	1.16	0.0284	1.09	1.59
200.1	2.96	0.0804	1.09	3.16

Table 8

RESULTS OF REPEATABILITY TESTING FOR DAM/CEREX AT $\bar{N}$ = 75 ℓ/IN

Original Test			Repeatability Test			% Difference
Mean Temp. (^{o}F)	K x 10^{5} $\frac{\text{Btu}}{\text{Hr-ft-}^{o}\text{F}}$	Probable Error + (%)	Mean Temp. (^{o}F)	K x 10^{5} $\frac{\text{Btu}}{\text{Hr-ft-}^{o}\text{F}}$	Probable Error ± (%)	In K
-190.1	2.29	1.45	-189.5	2.34	1.82	2.18
0.4	4.42	1.63	-1.0	4.43	2.13	0.226
198.8	13.03	1.87	196.2	13.34	1.50	2.38

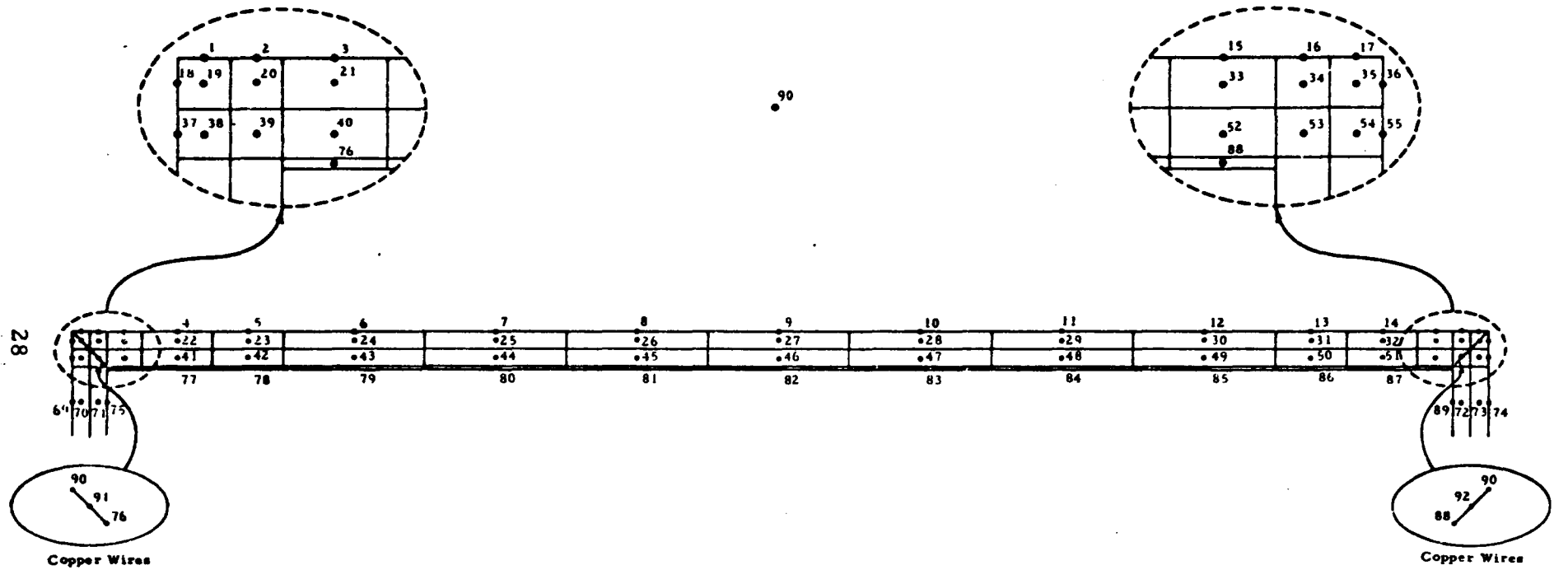

Fig. 1 - Nodal Network for Thermal Analysis of Lockheed's Cylindrical Calorimeter

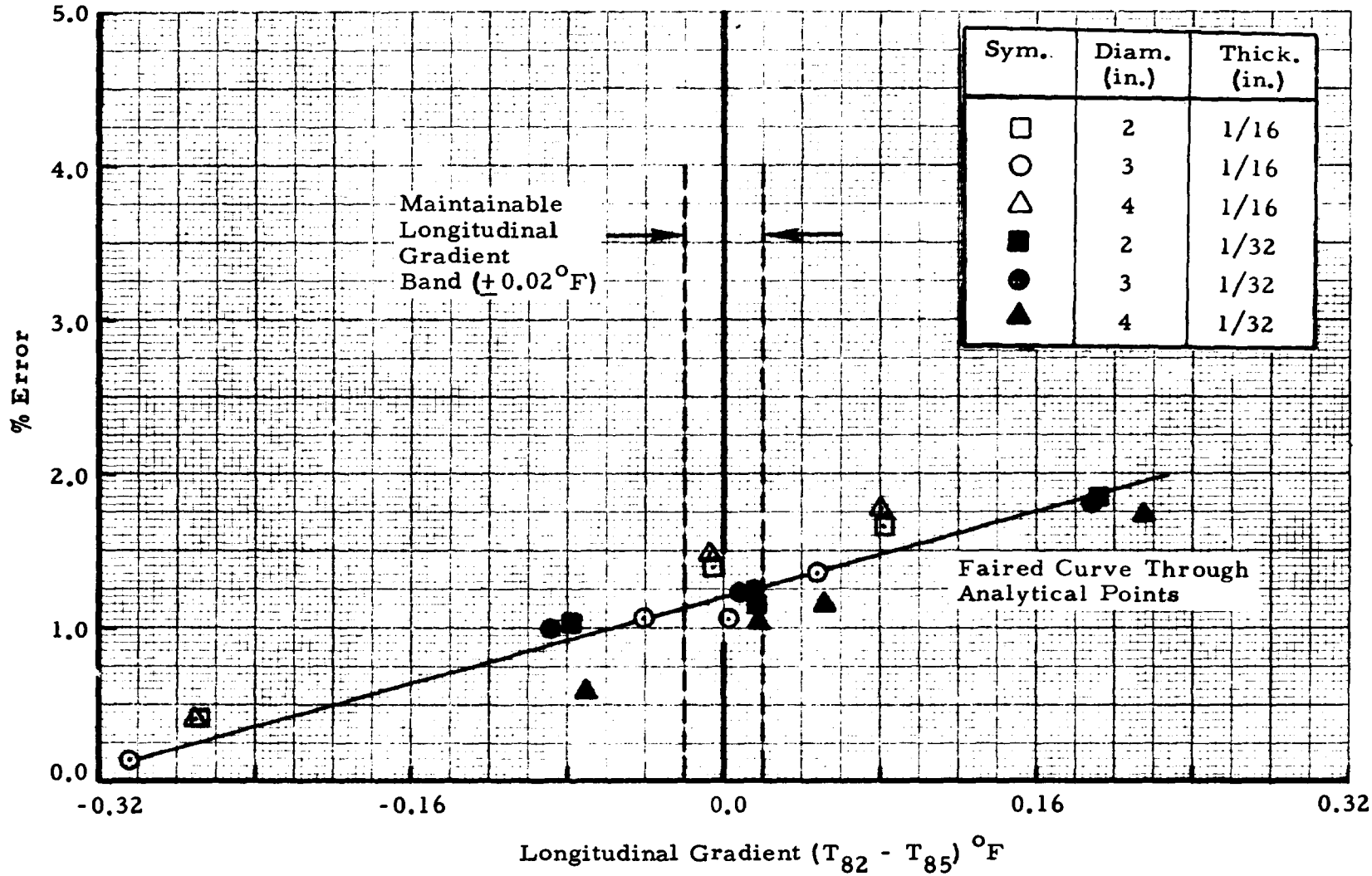

Fig. 2 - Error in Conductivity Measurement for Cylindrical Calorimeter with Internal Emissivity of Zero

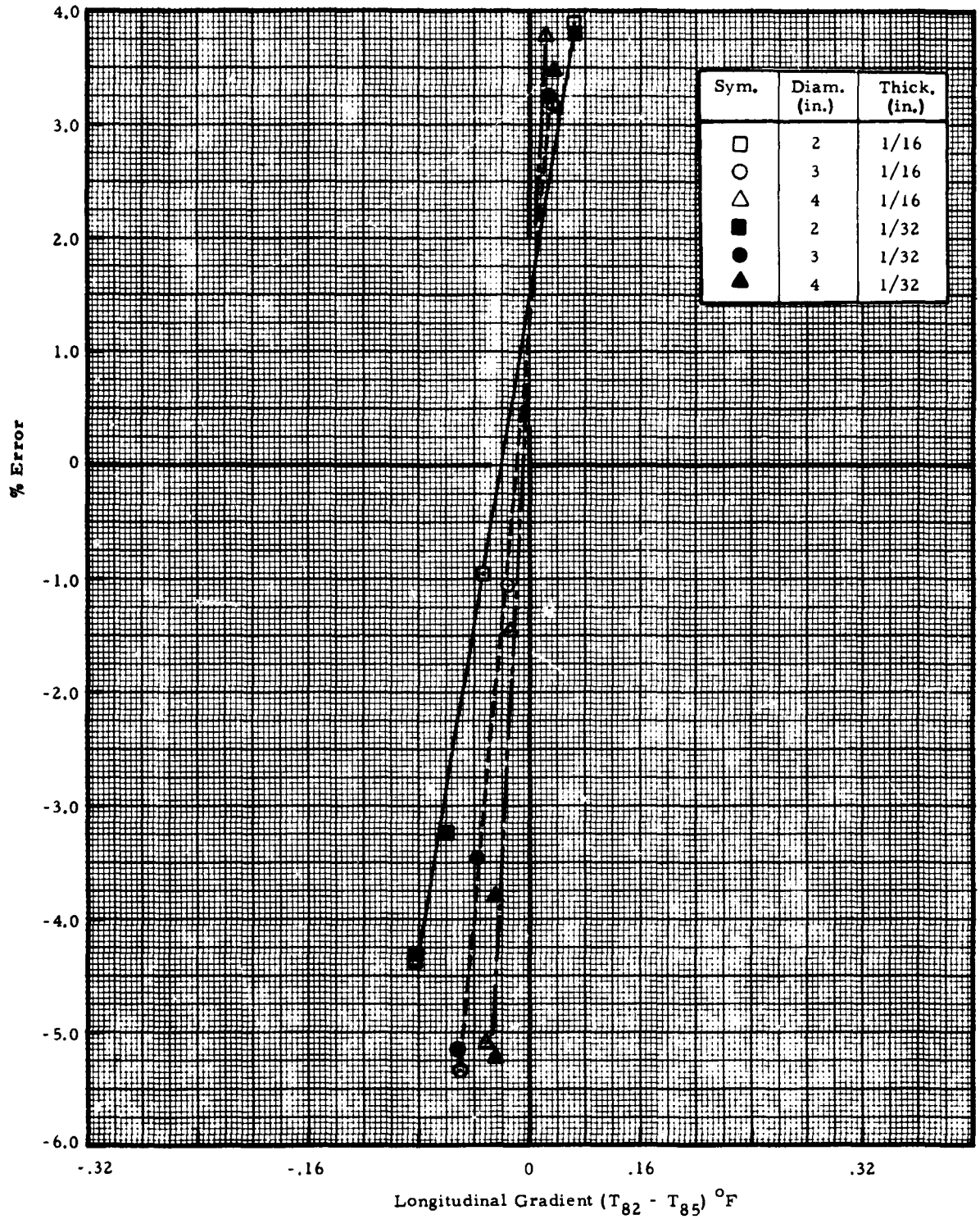

Fig. 3 - Error in Conductivity Measurement for Cylindrical Calorimeter with Internal Emissivity of 0.5

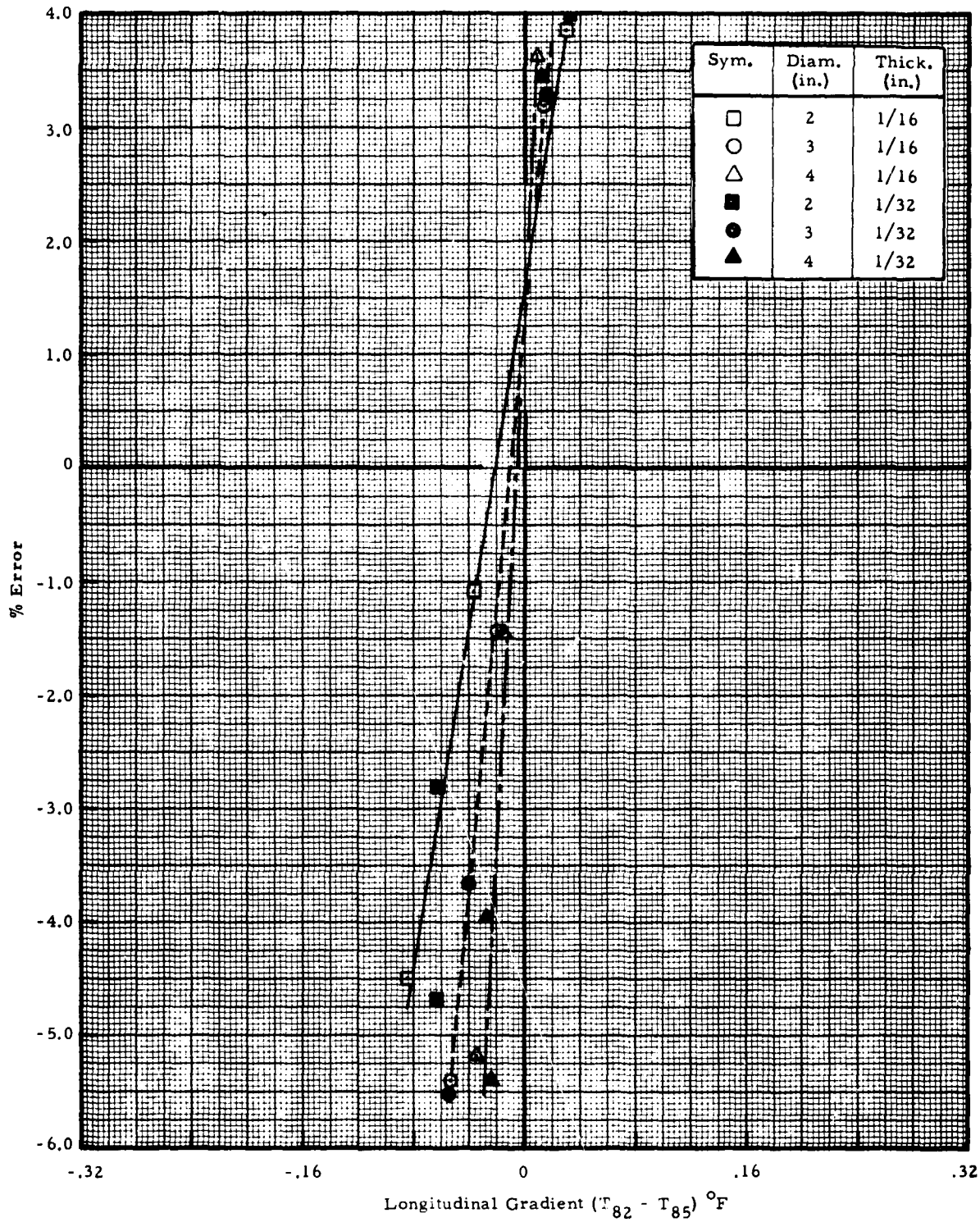

Fig. 4 - Error in Conductivity Measurement for Cylindrical Calorimeter with Internal Emissivity of 1.0

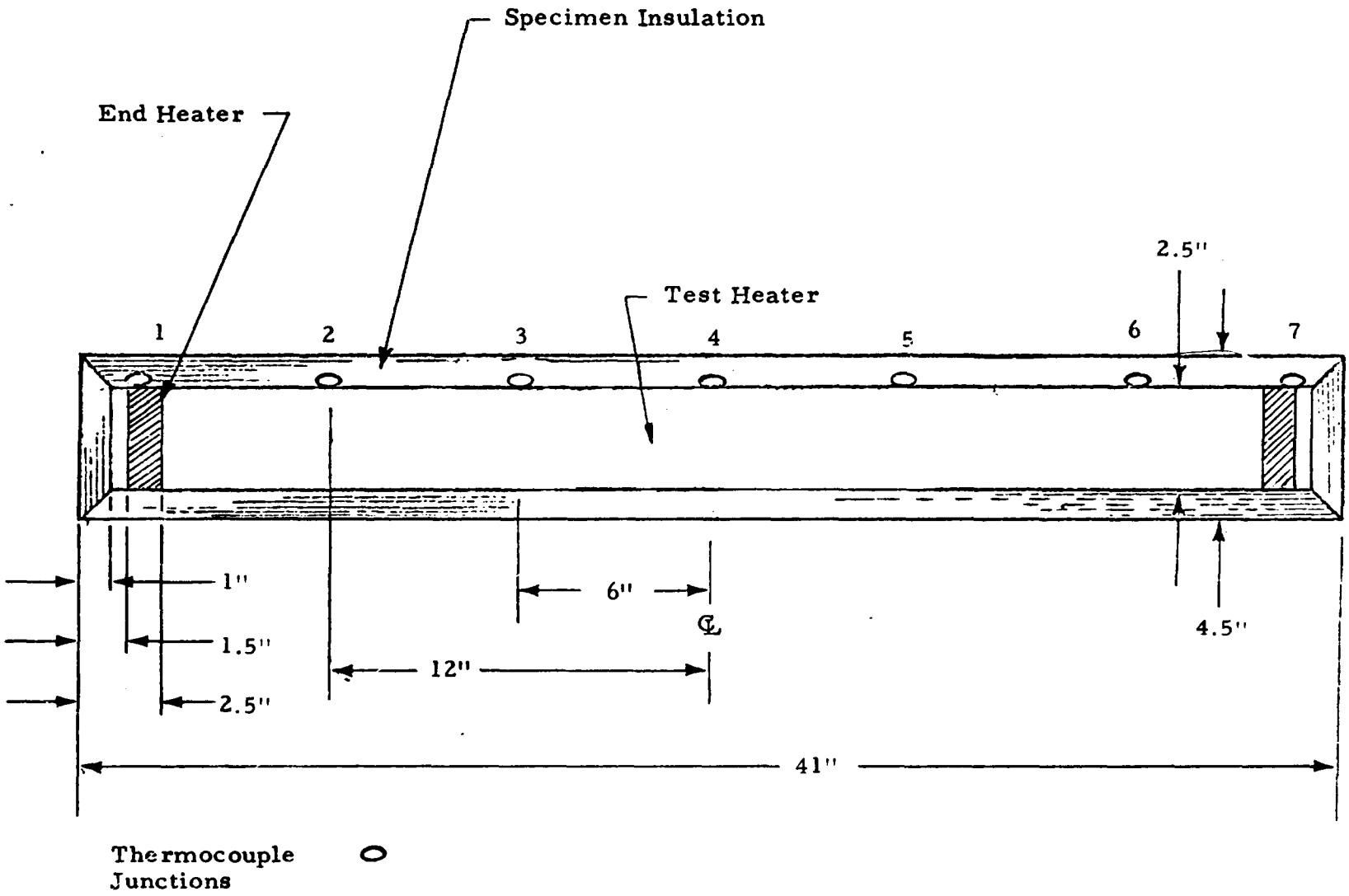

Fig. 5 - Schematic of Electrical Cylindrical Calorimeter

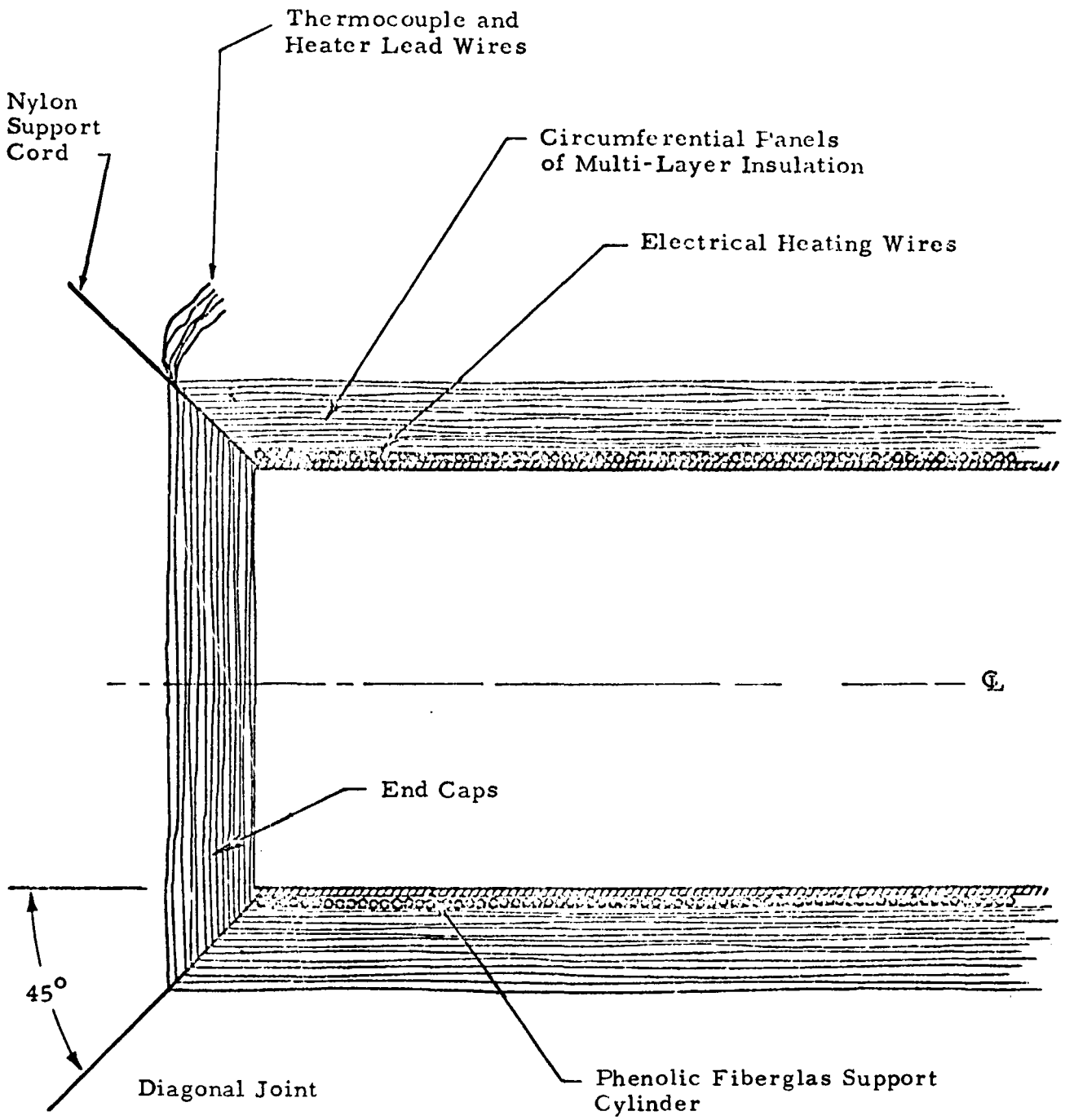

Fig. 6 - Insulation Application Concept

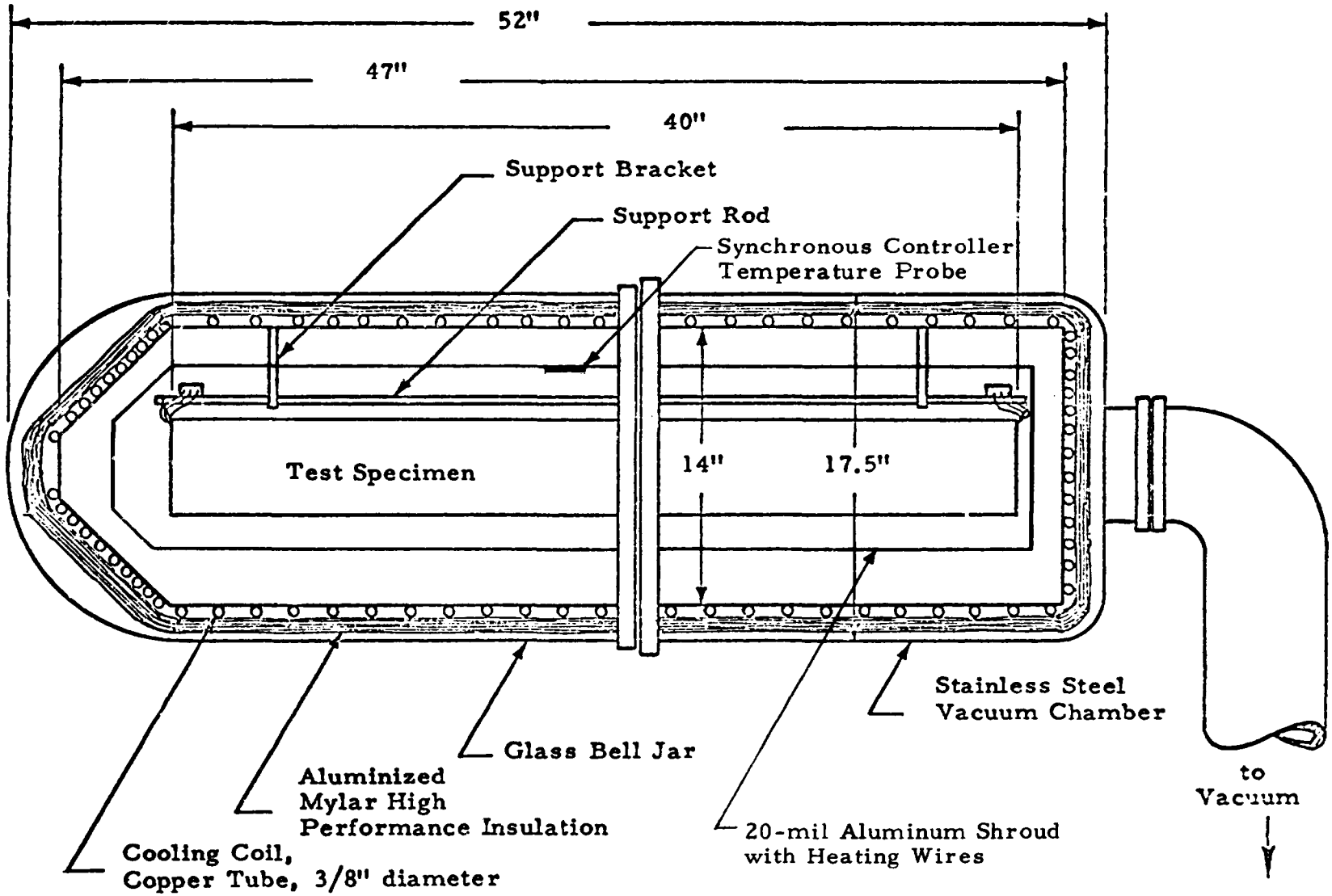

Fig. 7 - Environmental Control and Vacuum Chamber System

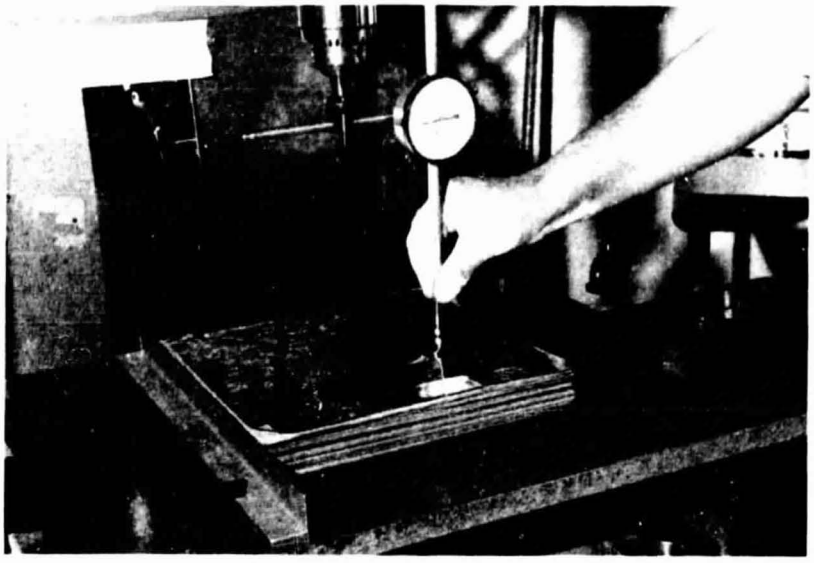

a. Unloaded

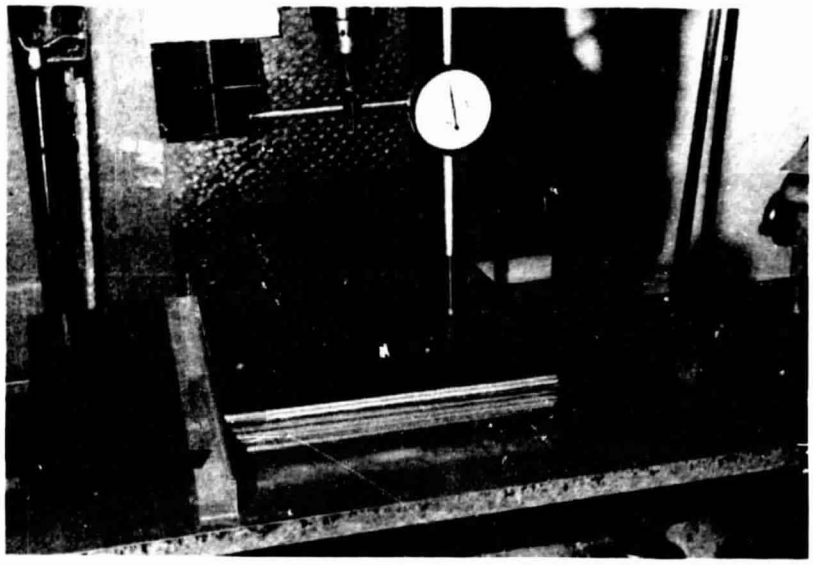

b. Loaded

Fig. 8 - Compression Test Apparatus

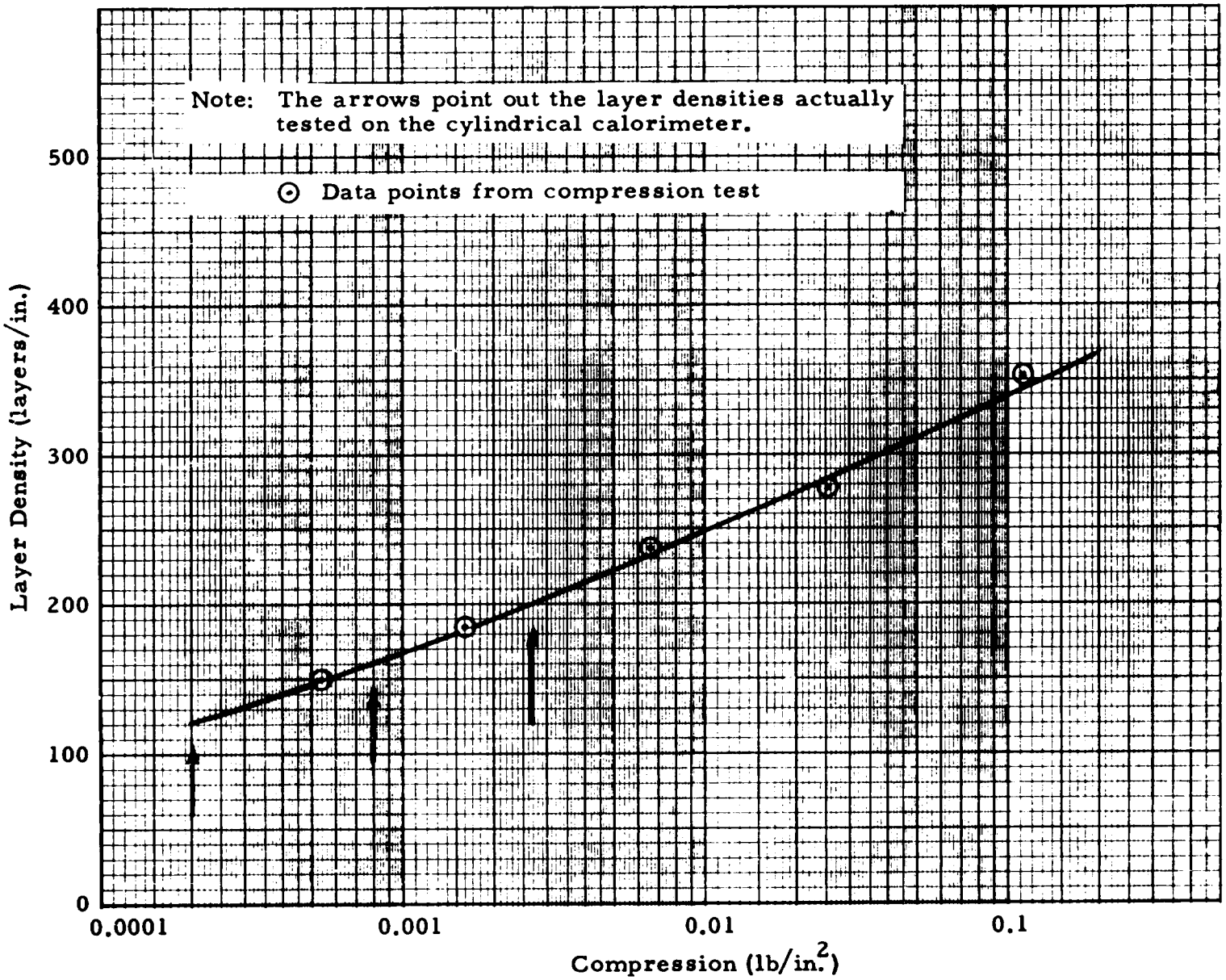

Fig. 9 - Compressibility Data for DAM/Tissuglas

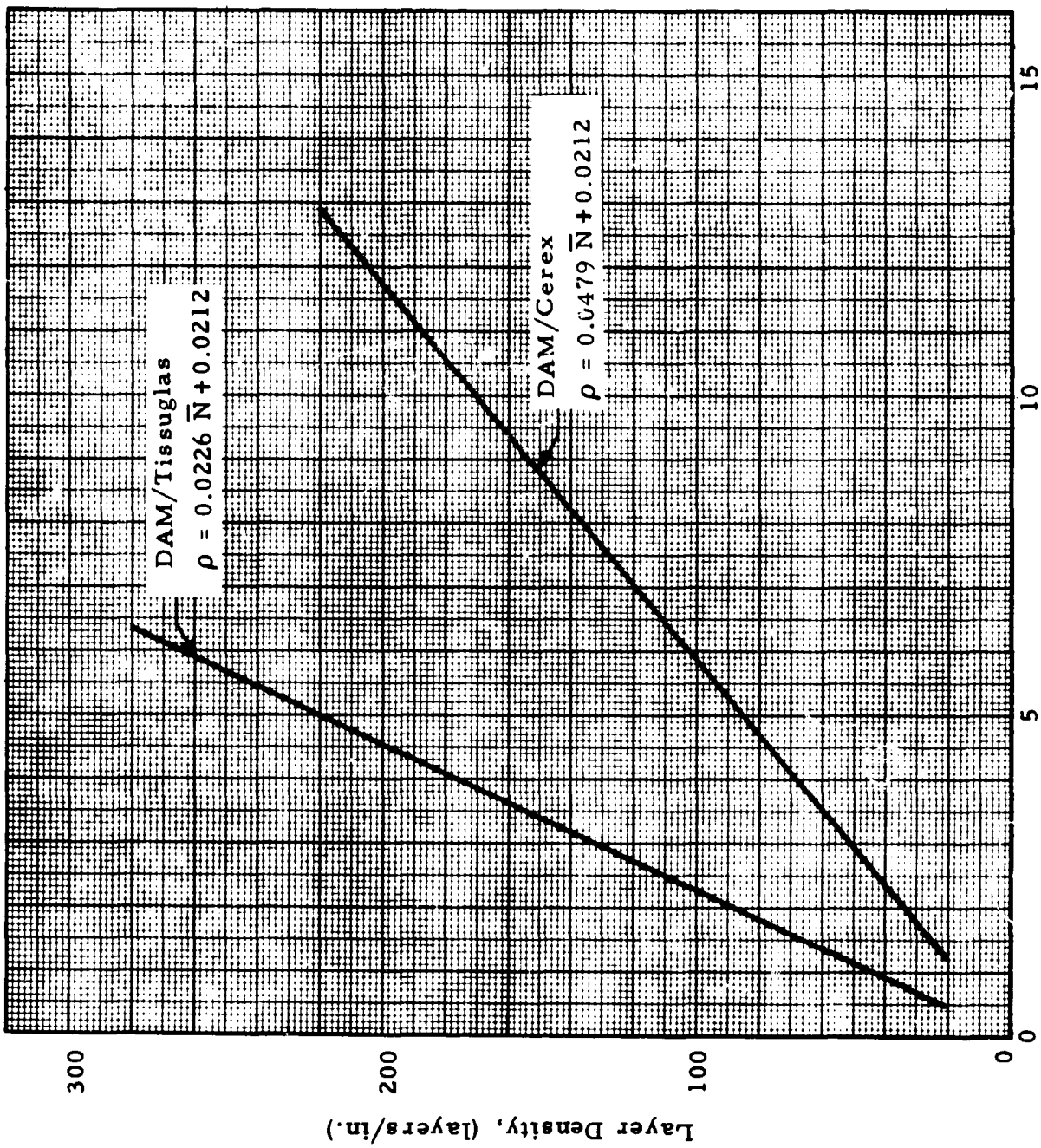

Fig. 10 - Density Data for DAM/Tissuglas and DAM/Cerex

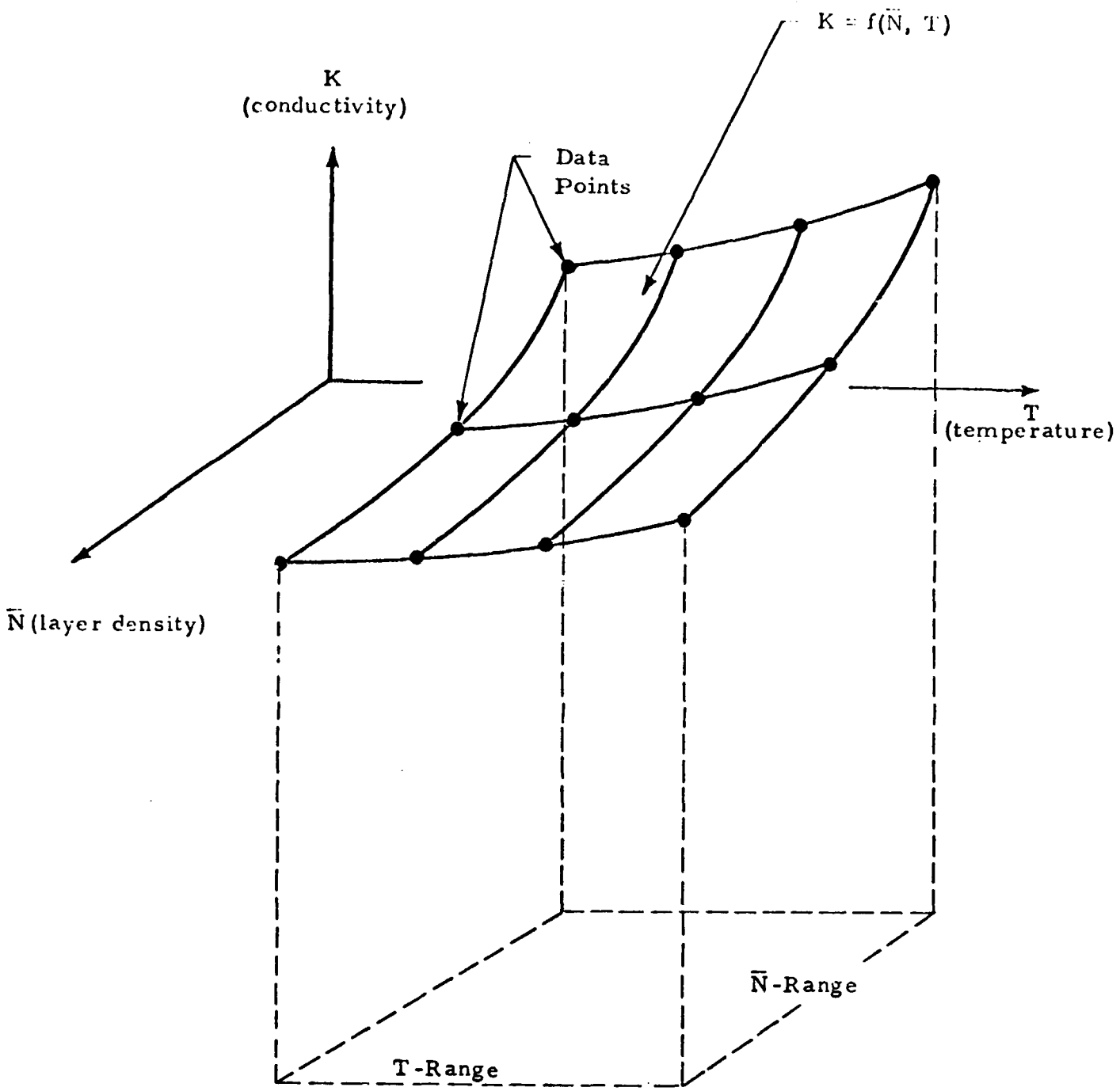

Fig. 11 - Data Surface for $K = f(T, \bar{N})$

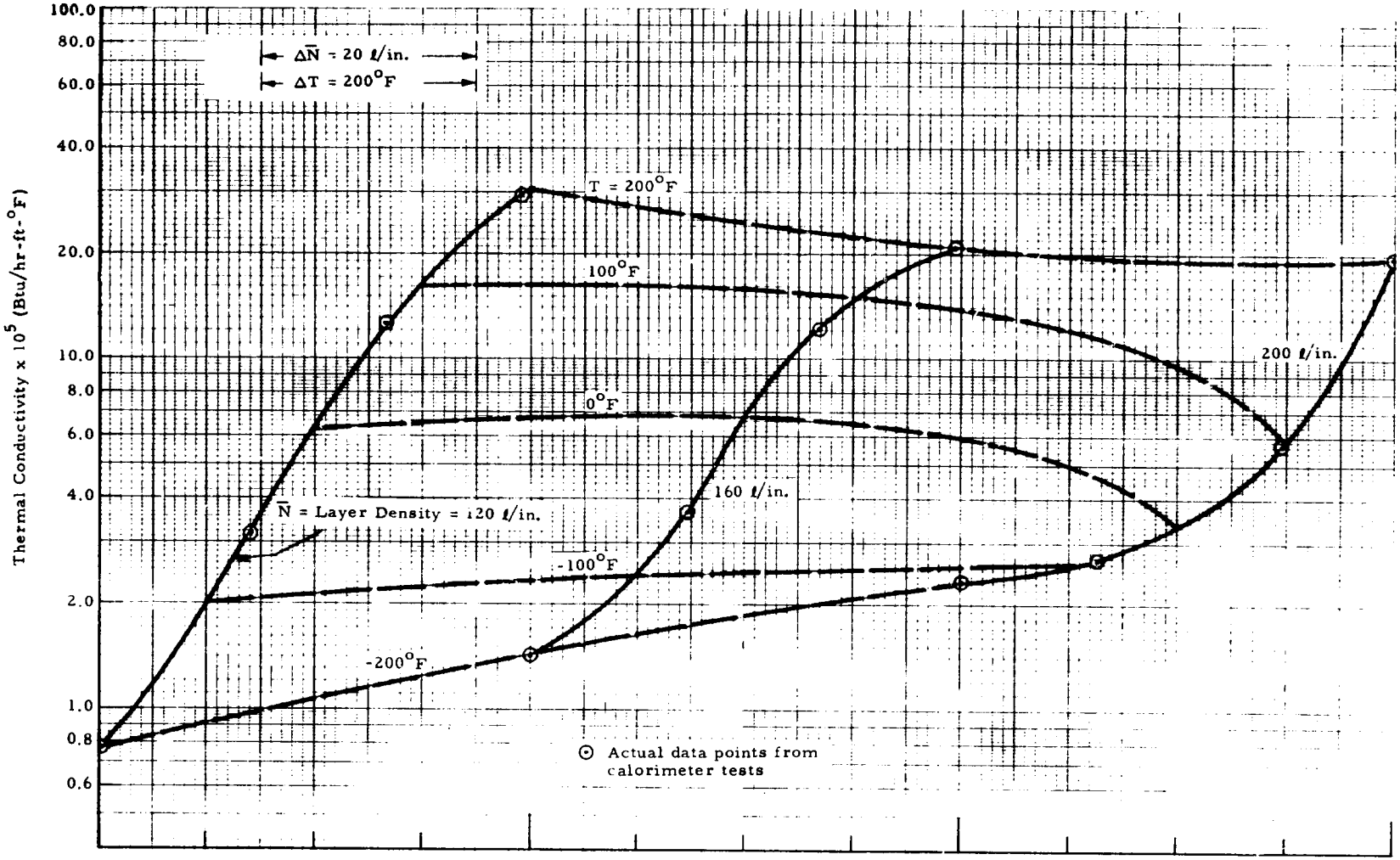

Fig. 12 - Thermal Conductivity Carpet Plot for DAM/Tissuglas

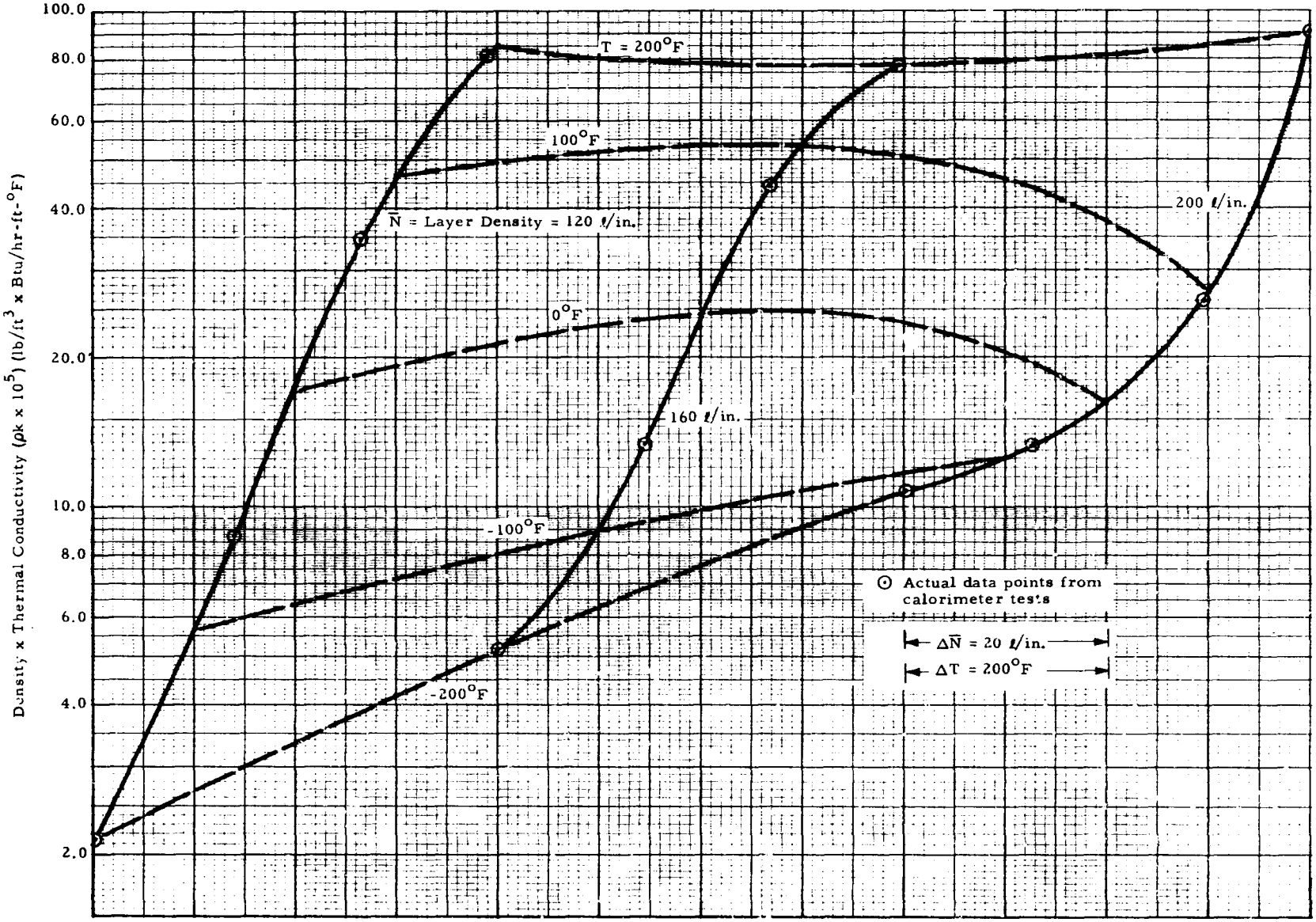

Fig. 13 - Density x Thermal Conductivity Carpet Plot for DAM/Tissuglas

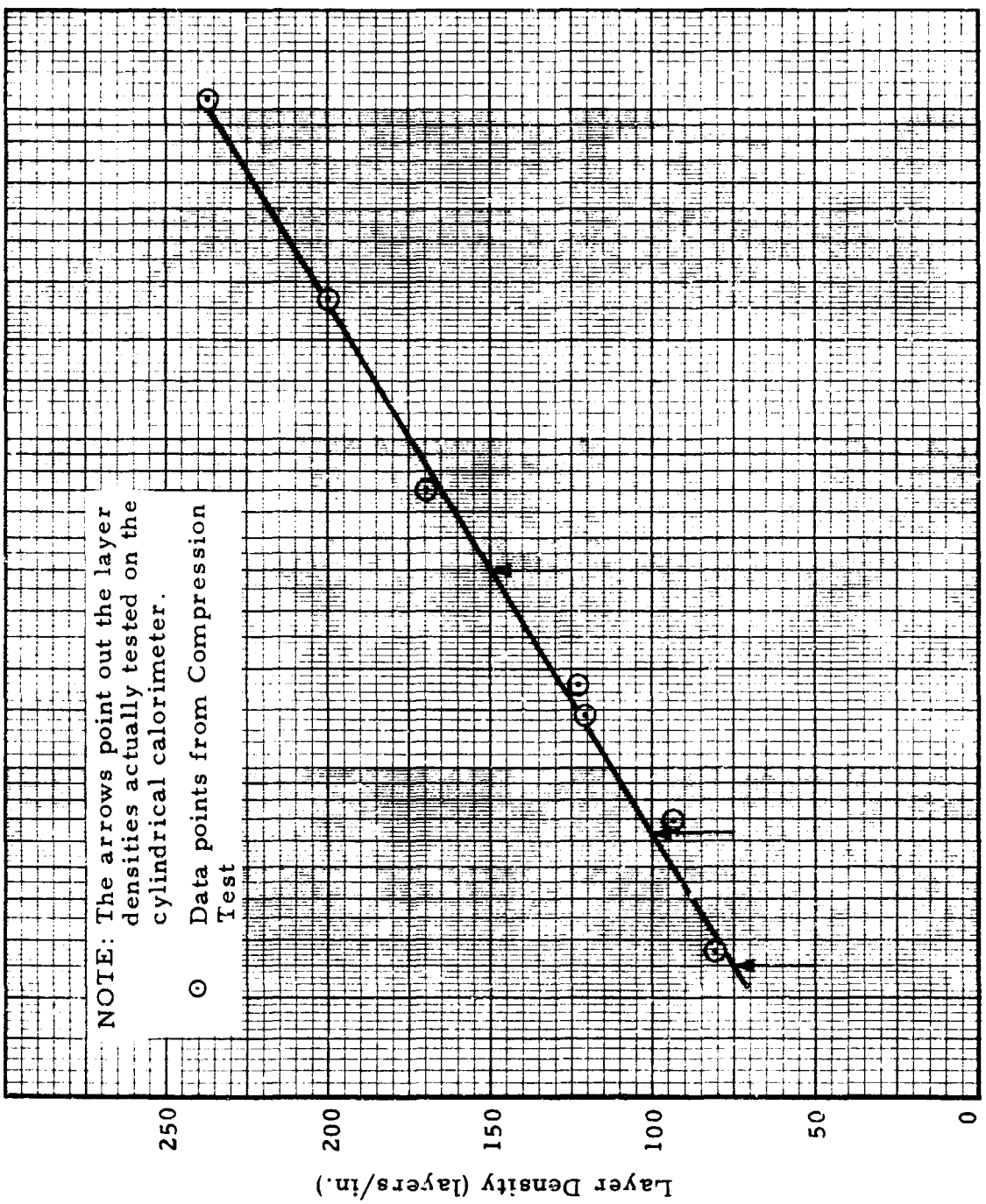

Fig. 14 - Compressibility Data for DAM/Cerex

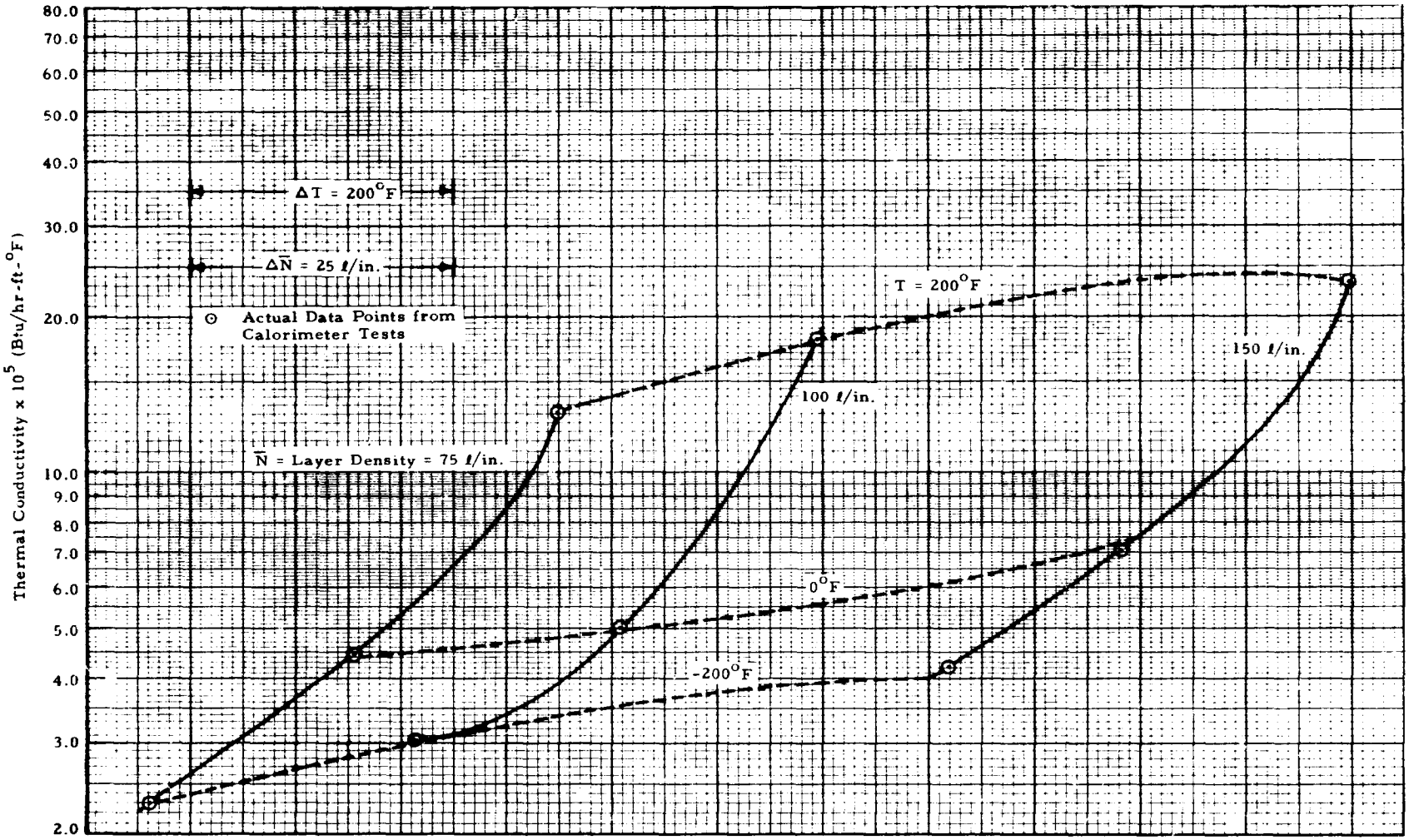

Fig. 15 - Thermal Conductivity Carpet Plot for DAM/Cerex

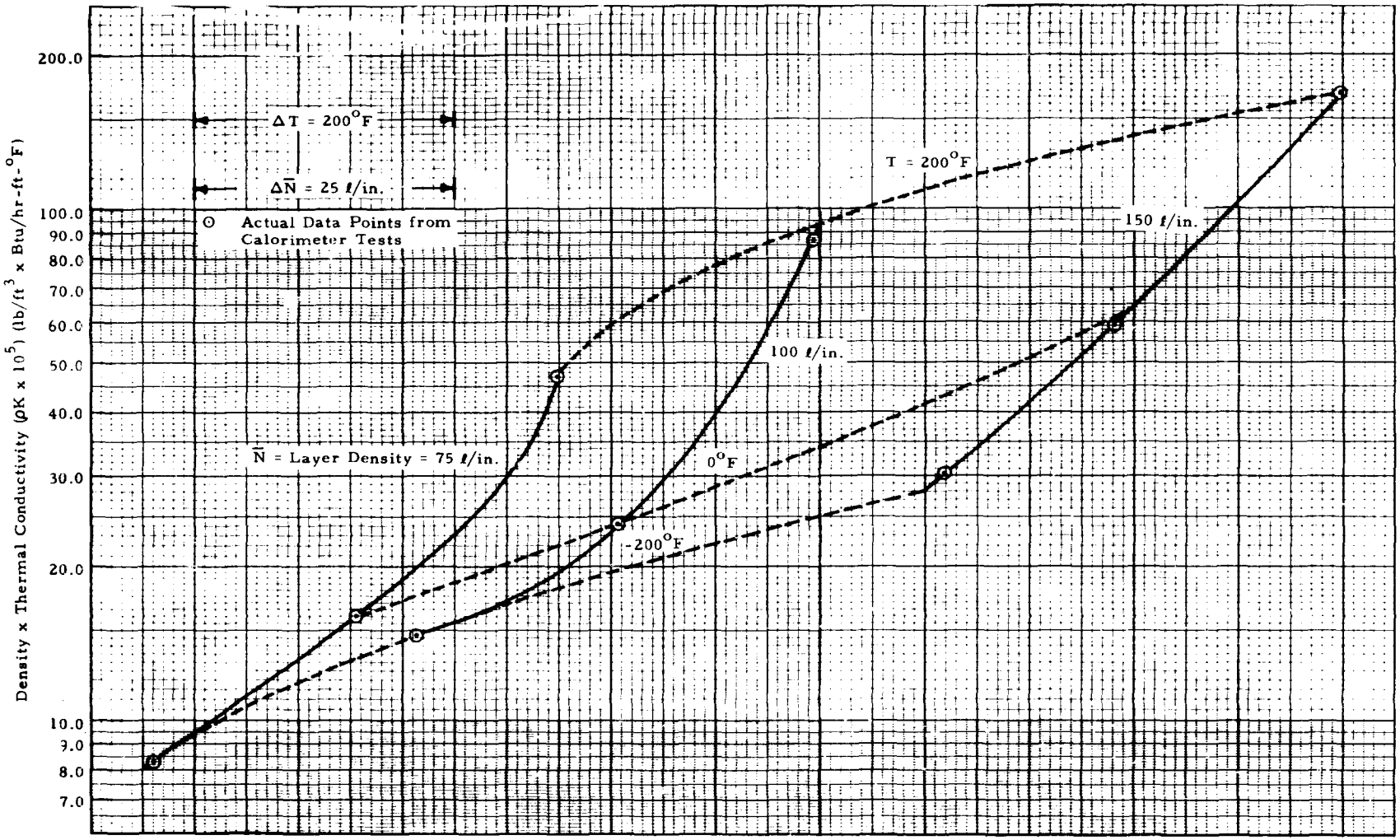

Fig. 16 - Density x Thermal Conductivity Carpet Plot for DAM/Cerex

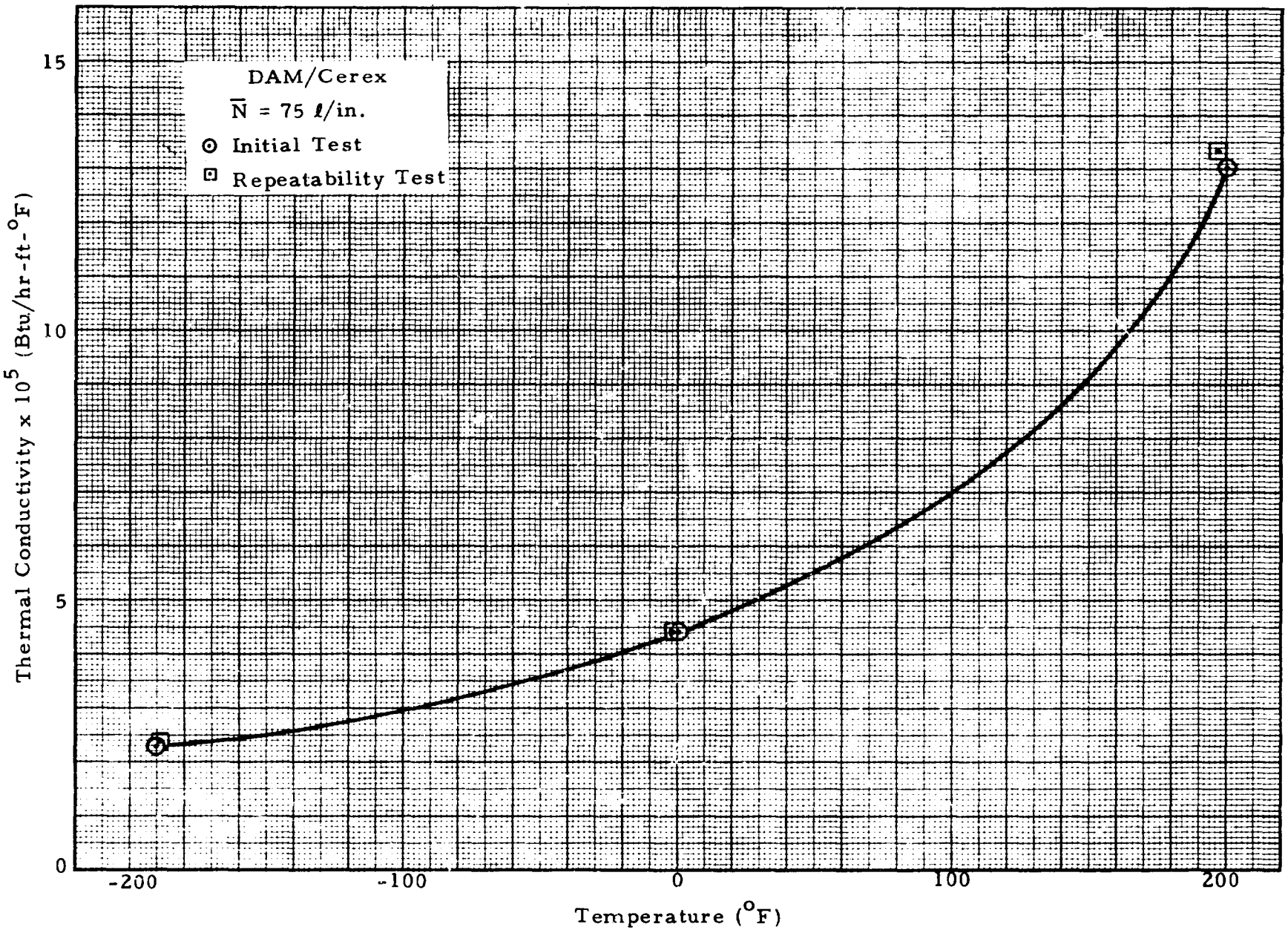

Fig. 17 - Thermal Conductivity Repeatability Test for DAM/Cerex

Appendix A

Given the carpet plot in Fig. A-1, in which ρK is shown as a function of T and $\overline{N}$, double interpolation can be used to obtain the ρK value for any set of T and $\overline{N}$ within the ranges of the plot. As an example, if it is desired to determine ρK for $\overline{N}$ = 140 ℓ/in. and T = -50°F, the following method should be used.

1. First, construct the $\overline{N}$ = 140 ℓ/in. curve. This is done by starting at intersection A. From the indicated scale, four large horizontal spaces represents 20 ℓ/in. Therefore, by moving to the right on curve AD a horizontal distance of four spaces, point 1 is located. The coordinates of point 1 are therefore (140 ℓ/in., -100°F). Similarly, starting at intersection B and traveling along curve BC four horizontal spaces to the right locates point 2. The coordinates of point 2 are therefore (140 ℓ/in., 0°F). A curve can now be faired through points 1 and 2 which should parallel AB and CD. This curve represents $\overline{N}$ = 140 ℓ/in.
2. Next, construct the T = -50°F curve. This is done by starting at intersection A. From the indicated scale, one large horizontal space represents 50°F. Therefore, by moving to the right on curve AB a horizontal distance of one space, point 3 is located. The coordinates of point 3 are therefore (120 ℓ/in., -50°F). Similarly, starting at intersection D and traveling along curve DC one horizontal space to the right locates point 4. The coordinates of point 4 are therefore (160 ℓ/in., -50°F). A curve can now be faired through points 3 and 4 which should parallel AD and BC. This curve represents T = -50°F.
3. The intersection (point 5) of curves 1-2 and 3-4 has the desired coordinates (140 ℓ-in., -50°F). The ρK value corresponding to this point can now be read directly from the abscissa, yielding the value:

$$\rho K = 12.5 \times 10^{-5} \text{ (lb/ft}^3\text{) x (Btu/hr-ft-}^\circ\text{F)}.$$

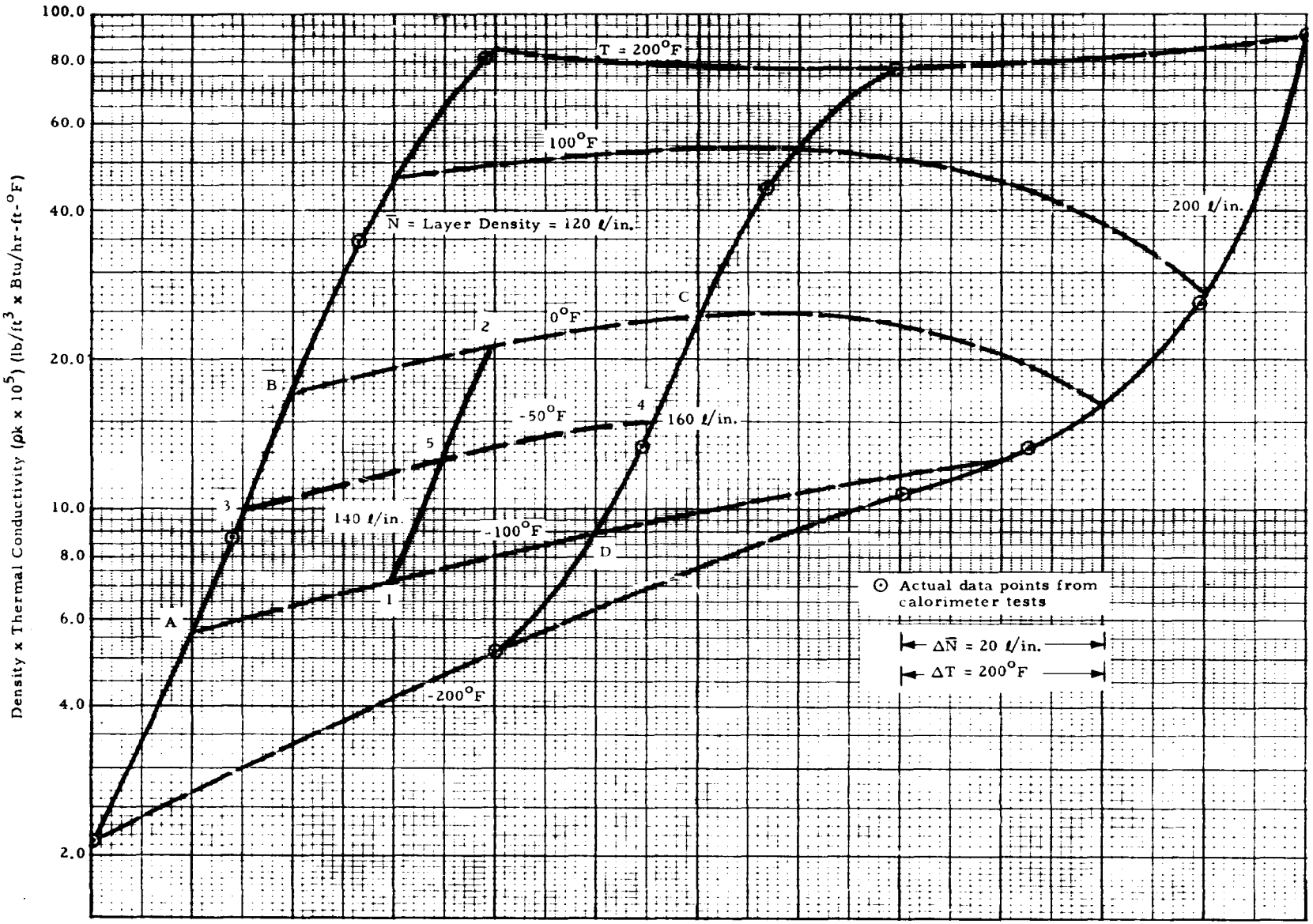

Fig. A-1 - Method for Double Interpolation on Carpet Plot